

### Supporting Information

Preparation of face-centered-cubic indium nanocubes and their superior dehydrogenation activity towards aqueous hydrazine with the assistance of light

Fang Luo,<sup>a,b</sup> Xue Miao,<sup>a,b</sup> Wei Chu,<sup>\*c</sup> Ping Wu<sup>a,b</sup> and Dong Ge Tong<sup>\*a,b</sup>

<sup>a</sup> Collaborative Innovation Center of Panxi Strategic Mineral Resources Multi-purpose Utilization, College of Materials and Chemistry & Chemical Engineering, Chengdu University of Technology, Chengdu 610059, China. E-mail: tongdongge@163.com; Fax: +86 28 8407 8940

<sup>b</sup> State Key Laboratory of Geohazard Prevention and Geoenvironment Protection (Chengdu University of Technology), Chengdu 610059, China.

<sup>c</sup> College of Chemical Engineering and Key Laboratory of Green Chemistry & Technology of Ministry of Education, Sichuan University, Chengdu 610065, China. E-mail: chuwei1965@foxmail.com; Fax: +86 28 8540 3397

Summary: 43 Pages; 3 Tables; 37 Figures

## Table of Contents

Experimental.....	4
Preparation of fcc-In nanocubes.....	4
Characterization.....	5
Catalytic dehydrogenation of aqueous hydrazine .....	6
3D-FDTD Simulation.....	7
Catalytic reduction of 4-nitroanisole .....	8
Photoelectrochemical performance measurements.....	8
Table S1 .....	10
Table S2 .....	11
Table S3 .....	13
Fig.S1 .....	18
Fig.S2 .....	18
Fig.S3 .....	19
Fig.S4 .....	20
Fig.S5 .....	21
Fig.S6 .....	23
Fig.S7 .....	23
Fig.S8 .....	24
Fig.S9 .....	25
Fig.S10.....	26
Fig.S11.....	26
Fig.S12.....	27
Fig.S13.....	28
Fig.S14.....	28
Fig.S15.....	29
Fig.S16.....	29
Fig.S17.....	30
Fig.S18.....	31
Fig.S19.....	32
Fig.S20.....	33
Fig.S21.....	34
Fig.S22.....	35
Fig.S23.....	36
Fig.S24.....	36
Fig.S25.....	37
Fig.S26.....	37
Fig.S27.....	38
Fig.S28.....	39
Fig.S29.....	39
Fig.S30.....	40
Fig.S31.....	40

Fig.S32.....	41
Fig.S33.....	41
Fig.S34.....	42
Fig.S35.....	42
Fig.S36.....	43
Fig.S37.....	43

## Experimental

### Preparation of fcc-In nanocubes

Anhydrous  $\text{InCl}_3$  were purchased from Sigma Aldrich and used as received. An in-house-designed reactor was used for the preparation of fcc In NCs via solution plasma technique. The tungsten electrodes were fixed in a Teflon vessel containing [BMIM]Cl, which served as a medium for the plasma reaction. The diameters of tungsten electrodes were 2 mm. Meanwhile, the inter-electrode distance was 0.5 mm. The applied discharge parameters were a potential of 200 V, a frequency of 6 kHz, a pulse duty of 25%, and an output current of 50 mA.

In a typical synthesis, 1 mmol  $\text{InCl}_3$  were mixed and dissolved in 30 mL [BMIM]Cl under hydrogen atmosphere. Then, 0.5 mmol  $\text{KClO}_4$  were added to the solution. No significant reaction occurred in the absence of plasma. After vigorous stirring for 30 min, SPT was carried out. The electric field of the plasma in the inter-electrode space was about  $400 \text{ Vcm}^{-1}$ . The precipitate was centrifuged and washed with ethanol and water. Finally, the obtained solid was treated via SPT in the solution of choline and urea (mole ratio =1:2) to desorb the  $\text{ClO}_4^-$ , and eventually was re-dispersed in hexane as a stable colloidal suspension before further use.

For comparison, conventional face-centered-cubic In NPs were prepared using the same procedure but without adding  $\text{ClO}_4^-$ . Body centered tetragonal (bct) In nanoparticles (NPs) were prepared according to the method reported by Cingarapu et al.<sup>10g</sup>

For the preparation of the fcc In /C, 106 mg of In NCs was dissolved in hexane in a 10 mL vial, and 26.5 mg of carbon (Vulcan XC-72R, Carbot, USA) support was carefully added to it. This colloidal mixture was stirred for 2 h to ensure complete adherence of the In NCs on the carbon support.

After the hexane evaporated, 5 mL of oxygen-free distilled water was added to the fcc In NCs/C dispersion, and the mixture was sonicated for 30 min to ensure uniform distribution. The aqueous fcc In NCs/C dispersion was protected in a sealed glass tube with a helium atmosphere. All catalytic reactions were performed using aqueous fcc In NCs/C catalyst dispersion; after experiments, the dispersion was transferred

into oxygen-free water and broken under water, to avoid the oxidation of fcc In NCs.

## **Characterization**

For compositional analyses, the dry samples were dissolved in boiling aqua fortis using a microwave digestion system. The In contents of the samples were determined using inductively coupled plasma atomic emission spectroscopy (ICP-AES; Iris, Advantage). Cl and O elemental analysis was carried out with a Vario Micro cube elemental analyzer. X-ray diffraction (XRD) patterns were recorded using an X'Pert X-ray powder diffractometer equipped with a CuK $\alpha$  radiation source ( $\lambda = 0.15406$  nm). The Brunauer–Emmett–Teller (BET)-specific surface area of the samples were determined using a N<sub>2</sub> adsorption–desorption method, during which the samples were degassed at 200°C for 180 min before the measurements.

Scanning transmission electron microscopy (STEM) images and selected-area electron diffraction patterns (SAED) of the samples were obtained with a JEOL-2100F microscope. Samples for STEM analysis were prepared by depositing a single drop of diluted nanoparticle dispersion in ethanol on an amorphous, carbon-coated copper grid. Fourier transform infrared spectra (FTIR) were collected using a Bruker FT-IR spectrometer (EQUINOX55). The surface electronic states of the samples were determined using X-ray photoelectron spectroscopy (XPS; Perkin–Elmer PHI 5000C ESCA, using AlK $\alpha$  radiation). The samples were fixed in a homemade *in situ* XPS reactor cell, and after drying under argon atmosphere, each sample was transferred to the analysis chamber and its XPS spectrum was recorded. All binding energies were referenced to the C1s peak (binding energy of 284.6eV) of the surface adventitious carbon. Time-of-flight secondary ion mass spectrometry (ToF-SIMS) experiments were carried out with a PHI TRIFT II (USA) equipped with a pulsed liquid metal ion gun. Spectra were obtained in positive ion mode over a mass range of 1–280Da using a Ga<sup>+</sup> primary source with a raster size of 100 × 100 mm<sup>2</sup>, applied voltage of 15 kV, aperture current of 600pA, and acquisition time of 10 min. At least three different spots on each sample were analyzed, and the most

representative data were used. Data acquisition and element composition analyses were carried out using the Ion-Spec software.

Ultraviolet–visible (UV–vis) spectra of  $\text{N}_2\text{H}_4$  were recorded using a UV5800 modal spectrophotometer. For the UV–vis measurements, a mixture of 0.5000 g of para-dimethylaminobenzaldehyde, 25.00 mL of ethanol, and 2.50 mL of hydrochloric acid ( $1.000 \text{ mol L}^{-1}$ ) was used as the chromogenic agent for  $\text{N}_2\text{H}_4$ . Next, 0.30 mL hydrous hydrazine solution, 0.10 mL of the chromogenic agent, and 3.40 mL of deionized water were mixed together and stored for 30 min before being tested. The calibration curve was shown in Fig. S21.

UV–vis spectra of In NPs were recorded with a Varian Cary Scan 100. For this purpose, two drops of the as-prepared In NPs suspensions were diluted with 4 mL of diethylene glycol. Measurements were performed in transmission geometry using quartz cuvettes.

The ion motilities of various anions in [BMIM]Cl were determined in a home-made electrolytic cell (200 mm in length, 75 mm in width, and 60 mm in height) via an isotope tracer method. Tungsten plates ( $20 \text{ mm} \times 20 \text{ mm}$ ) were used as the two electrodes. The measurement of radioactive isotopes was conducted using a scintillation counter (Phonix, NIPC, Chengdu, China), while the analysis of stable isotopes was performed on a MAT 253 isotope mass spectrometer (Thermo Fisher Scientific, USA).

The attenuated total reflectance Fourier transform infrared (ATR-FTIR) spectra were recorded at  $25 \text{ }^\circ\text{C}$  by a FTIR spectrometer (PerkinElmer, MA, USA) attached the general ATR sampling accessory (PerkinElmer, MA, USA). The diamond/ZnSe trapezoidal IRE ATR crystal has a refractive index of 2.417. The incidence angle is  $45^\circ$ , giving three reflections in contact with the sample. The series of spectra were measured at  $4 \text{ cm}^{-1}$  resolution with eight scans. The wavenumber range was from 4000 to  $400 \text{ cm}^{-1}$ .

### **Catalytic dehydrogenation of aqueous hydrazine**

The performance of the samples for aqueous hydrazine dehydrogenation was

determined by measuring the hydrogen release rate of the reaction with an on-line gas chromatography system (GC, HP Series 68900, Palo Alto, CA, USA), which is equipped with a 13X column and a thermal conductivity detector. The gas effluent was carried to the GC by flowing Ar carrier gas at 100 sccm through the flask reactor. The peak areas of the H<sub>2</sub> and N<sub>2</sub> were calibrated for a standard gas mixture with a molar ratio H<sub>2</sub>:N<sub>2</sub> = 2:1. The calibration curves were shown in Figs. S16 and S17. Both of the calibration curves show excellent linearity with coefficients greater than 0.999.

The reaction was initiated via the introduction of aqueous hydrazine into a three-neck round-bottom flask containing the as-prepared catalyst under magnetic stirring. The gas generated during the reaction was passed through a trap containing 0.01000 mol L<sup>-1</sup> HCl standardized solution at room temperature to ensure the absorption of any ammonia generated. After the gas release stopped, the obtained solution was titrated with a standard solution of 0.01000 mol L<sup>-1</sup> NaOH using phenolphthalein as an acid–base indicator. The amount of ammonia gas generated was determined from the difference in concentration between the HCl solution before and after the reaction. For mass spectral analyses, the acid trap was not used. The ion source temperature of the mass spectrometer (DeltaPLUS; Finnigan MAT, Bremen, Germany) was 200°C, the ionization energy was 70 eV, and the scan rate was 2.78 (single ion monitor). The detection limits were 33 ppb for H<sub>2</sub>, 18 ppb for N<sub>2</sub>, and 10 ppb for NH<sub>3</sub>.

For light-enhanced hydrogen generation, we irradiated the above reaction mixture with a 500 W Xe lamp at a fixed power density of 95 mW cm<sup>-2</sup>.

The catalyst was recovered via centrifugation, and was then washed thoroughly (at least three times) with water and absolute ethanol. Followed by drying overnight at 60 °C, the sample was then reused for the hydrogen evolution reaction from aqueous hydrazine with the assistance of light.

### **3D-FDTD Simulation.**

Numerical simulations using the finite-difference time-domain method (FDTD

Solutions, Nano Mater Solutions) were carried out to simulate the extinction spectra of nanostructures. The refractive index of the medium was set to be 1.33, as all the nanoparticles were dispersed in water. In the simulations, all the space in x, y, and z directions were set to be 0.1  $\mu\text{m}$ . Dimensions of nanocrystals were adopted those determined from the STEM images. The boundaries of the simulation volume were perfectly matched layers (PML). They are 100 nm away from the center of nanocubes.

For easy observation, a normal-incident plane wave source illuminates the nanocubes along the z axis without any tilt angle. The 2D plane was at the nanocube center in the xy plane. The observed 2D profile, which is the function of near electric field intensity ( $|E_x|^2 + |E_y|^2 + |E_z|^2$ ) and positions of x and y axes, was then recorded.

### **Catalytic reduction of 4-nitroanisole**

106 mg 6.8nm fcc-In nanocubes (80% wt.) loaded on 26.5 mg carbon and 4-nitroanisole (0.25 mol) was then added in a three-neck round-bottom flask. After stirring thoroughly, 100 mL of 5.0 molL<sup>-1</sup> hydrazine solution was added and start the reaction. The reaction products was then analyzed using a GC (GC-2014, Shimadzu) equipped with an FID and a capillary column (DM-WAX, 30 m  $\times$  0.32 mm  $\times$  0.25 mm, Dikma). The response factors of each component were determined with standard samples and used to calculate the conversion and selectivity. To further investigate the photocatalytic rate enhancement, we carried out the same reaction in the presence of a 500 W Xe lamp at a power density 95 mWcm<sup>-2</sup> keeping other parameters constant.

### **Photoelectrochemical performance measurements**

To prepare the working electrode for the photoelectrochemical experiments, 10 mg samples were mixed with the solution of Nafion and ethanol (volume ratio=1:9) to obtain a paste. The resulting composite was supported on a 4 cm<sup>2</sup> conductive glass and then heated to 60 °C in an oven for 24 hours under vacuum.

The photoelectrochemical measurements were performed using a classical three-electrode cell consisting of the photoanode (working electrode), Pt counter

electrode and a saturated calomel reference electrode (SCE). The photocurrent response was recorded on a CHI 660C electrochemical workstation (the current density was normalized by the geometric surface area of the electrode) using 0.2 M NaCl as the electrolyte solution. The working electrode was irradiated by a 500 W Xenon lamp at a power density  $95 \text{ mWcm}^{-2}$  with an optical pass filter ( $\lambda > 420 \text{ nm}$ ).

**Table S1.** Ion motilities of different anions in ionic liquid [BMIM]Cl

Samples	Used isotope	Measured approach	Anions/ molL <sup>-1</sup>	Electric Vcm <sup>-1</sup>	field/ Test time / min	Ion motilities / 10 <sup>-7</sup> m <sup>2</sup> V <sup>-1</sup> s <sup>-1</sup>
ClO <sub>4</sub> <sup>-</sup>	<sup>35</sup> Cl	Isotope spectrometer	mass 0.01	40	30	1.9
ClO <sub>4</sub> <sup>-</sup>	<sup>35</sup> Cl	Isotope spectrometer	mass 0.01	100	30	1.9
ClO <sub>4</sub> <sup>-</sup>	<sup>35</sup> Cl	Isotope spectrometer	mass 0.01	400*	30	2.0
ClO <sub>4</sub> <sup>-</sup>	<sup>35</sup> Cl	Isotope spectrometer	mass 0.01	1000	30	1.9
ClO <sub>4</sub> <sup>-</sup>	<sup>35</sup> Cl	Isotope spectrometer	mass 0.001	400*	30	2.0
SO <sub>4</sub> <sup>2-</sup>	<sup>34</sup> S	Scintillation counter	0.01	400*	30	3.9
PO <sub>4</sub> <sup>3-</sup>	<sup>32</sup> P	Scintillation counter	0.01	400*	30	4.8
PO <sub>3</sub> <sup>3-</sup>	<sup>32</sup> P	Scintillation counter	0.01	400*	30	6.0
Br <sup>-</sup>	<sup>81</sup> Br	Isotope spectrometer	mass 0.01	400*	30	2.5
I <sup>-</sup>	<sup>131</sup> I	Scintillation counter	0.01	400*	30	2.3
NO <sub>3</sub> <sup>-</sup>	<sup>15</sup> N	Isotope spectrometer	mass 0.01	400*	30	2.7

\*The electric field intensity is the same as that of SPT in this work.

**Table S2** The effect of reaction parameters, including plasma power, reaction temperature, reaction time, KClO<sub>4</sub> amounts, In precursors, Ionic liquids (Ils) volume, H<sub>2</sub> rate on the cube percentage, average diameter and phase composition of fcc-In nanocubes prepared with SPT.

Sample	Reaction temperature/ °C	Reaction time /min	Plasma power /W	KClO <sub>4</sub> amounts/mmol	Ils volume/mL	H <sub>2</sub> rate/mLmin. <sub>1</sub>	Cube percentage /%	Average edge length /nm	Phase composition
1	50	10	10	0.5	30	5	100	13.2	fcc
2	40	10	10	0.5	30	5	100	11.1	fcc
3	30	10	10	0.5	30	5	100	8.9	fcc
4	25	10	10	0.5	30	5	100	6.8	fcc
5	20	10	10	0.5	30	5	80.1	6.0	fcc
6	15	10	10	0.5	30	5	65.3	5.5	fcc
7	25	1	10	0.5	30	5	0	2.5	fcc
8	25	2	10	0.5	30	5	30.6	4.3	fcc
9	25	5	10	0.5	30	5	80.4	5.5	fcc
10	25	30	10	0.5	30	5	100	6.8	fcc
11	25	10	7	0.5	30	5	No products	-	-
12	25	10	15	0.5	30	5	100	8.9	fcc
13	25	10	20	0.5	30	5	100	12.2	fcc
14	25	10	30	0.5	30	5	100	15.5	fcc
15	25	10	10	0.1	30	5	84.1	3.1	fcc
16	25	10	10	0.3	30	5	93.8	5.0	fcc
17	25	10	10	1.0	30	5	100	6.8	fcc
18	25	10	10	0.5	50	5	100	6.8	fcc
19	25	10	10	0.5	100	5	100	6.8	fcc
20	25	10	10	0.5	30	1	88.1	4.5	fcc
21	25	10	10	0.5	30	3	93.7	5.7	fcc

---

22	25	10	10	0.5	30	8	100	8.7	fcc
23	25	10	10	0.5	30	10	95.0	9.5	fcc

---

**Table S3.** Catalytic activities of different catalysts for the dehydrogenation of hydrazine in aqueous solution

Samples	Specific surface area / $\text{m}^2 \text{g}^{-1}$	Temperature / K	Light * or not	$\text{H}_2$ generation volume / mL	$\text{H}_2$ selectivity / %	Time / min	TOF / $\text{mol H}_2 \text{mol}^{-1} \text{catalyst min}^{-1}$
6.8 nm fcc-In NCs	84.1	298	Light	$22.4 \times 10^3$	100	9.9	110
6.8 nm fcc-In NCs	84.1	298	Without light	$17.9 \times 10^3$	80.0	108	8.0
6.8 nm fcc-In NCs loaded on C (80 wt.%) in this work	204.1	298	Light	$22.4 \times 10^3$	100	6.3	172
6.8 nm fcc-In NCs loaded on C (80 wt.%) in this work	204.1	298	Without light	$17.9 \times 10^3$	80.0	65	13.3
8.9 nm fcc-In NCs in this work	76.5	298	Light	$22.4 \times 10^3$	100	11.7	92.7
8.9 nm fcc-In NCs in this work	76.5	298	Without light	$16.9 \times 10^3$	75.5	141.9	5.7
8.9 nm fcc-In NCs loaded on C (80 wt.%) in this work	179.1	298	Light	$22.4 \times 10^3$	100	7.8	139
8.9 nm fcc-In NCs loaded on C (80 wt.%) in this work	179.1	298	Without light	$16.9 \times 10^3$	75.5	87.6	9.3
11.1nm fcc-In NCs in this work	70.6	298	Light	$22.4 \times 10^3$	100	16	67.5
11.1nm fcc-In NCs in this work	70.6	298	Without light	$15.7 \times 10^3$	70.0	171	4.4
11.1nm fcc-In NCs loaded on C (80 wt.%) in this work	167.4	298	Light	$22.4 \times 10^3$	100	10	108
11.1nm fcc-In NCs loaded on C (80 wt.%) in this work	167.4	298	Without light	$15.7 \times 10^3$	70.0	105	7.2
13.2nm fcc-In NCs in this work	64.2	298	Light	$22.4 \times 10^3$	100	22.4	48.4

13.2nm fcc-In NCs in this work	64.2	298	Without light	$15.0 \times 10^3$	67.2	215	3.4
13.2nm fcc-In NCs loaded on C (80 wt.%) in this work	160.7	298	Light	$22.4 \times 10^3$	100	13.8	78.5
13.2nm fcc-In NCs loaded on C (80 wt.%) in this work	160.7	298	Without light	$15.0 \times 10^3$	67.2	133	5.5
15.5nm fcc-In NCs loaded on C (80 wt.%) in this work	56.7	298	Light	$22.4 \times 10^3$	100	29.7	38.2
15.5nm fcc-In NCs loaded on C (80 wt.%) in this work	56.7	298	Without light	$14.5 \times 10^3$	65.0	272	2.6
15.5nm fcc-In NCs loaded on C (80 wt.%) in this work	150.3	298	Light	$22.4 \times 10^3$	100	18.1	62.7
15.5nm fcc-In NCs loaded on C (80 wt.%) in this work	150.3	298	Without light	$14.5 \times 10^3$	65.0	165	4.3
conventional fcc-In NPs in this work	27.6	298	Light	$18.1 \times 10^3$	80.9	146	6.0
conventional fcc-In NPs in this work	27.6	298	Without light	$13.5 \times 10^3$	60.1	804	0.81
conventional fcc-In NPs loaded on C (80 wt.%) in this work	110.8	298	Light	$18.1 \times 10^3$	80.9	85.9	10.2
conventional fcc-In NPs loaded on C (80 wt.%) in this work	110.8	298	Without light	$13.5 \times 10^3$	60.1	465	1.4
conventional bct-In NPs in this work	30.1	298	Light	$9.4 \times 10^3$	41.8	4530	0.1
conventional bct-In NPs in this work	30.1	298	Without light	$4.9 \times 10^3$	21.8	11810	0.02

conventional bct-In NPs loaded on C (80 wt.%) in this work	116.9	298	Light	$9.4 \times 10^3$	41.8	1510	0.3
conventional bct-In NPs loaded on C (80 wt.%) in this work	116.9	298	Without light	$4.9 \times 10^3$	21.8	4724	0.05
fcc-In <sub>4</sub> Ni NRs <sup>7b</sup>	-	298	Without light	2240.0	100.0	15.5	83.6
In situ Rh <sub>4</sub> Ni <sup>6a</sup>	-	298	Without light	89.6	100.0	160	0.25
In situ Ni <sub>0.93</sub> Pt <sub>0.07</sub> <sup>2c</sup>	-	298	Without light	89.6	100.0	190	0.0021
In situ Ni <sub>0.95</sub> Ir <sub>0.05</sub> <sup>2d</sup>	-	298	Without light	89.6	100.0	390	0.26
Co-B nanospheres <sup>3a</sup>	-	298	Without light	954.2	21.3	23	5.34
Ni-Al <sub>2</sub> O <sub>3</sub> -HT <sup>6b</sup>	-	303	Without light	-	93.0	70	0.033
Co-B honeycomb <sup>3b</sup>	-	298	Without light	1872.6	41.8	13	12.6
NiPt <sub>0.057</sub> /Al <sub>2</sub> O <sub>3</sub> <sup>3e</sup>	-	303	Without light	70.2	98.0	11.5	0.28
Mondispersed Ni <sub>3</sub> Fe nanospheres /C <sup>3c</sup>	-	293	Without light	224.0	100.0	27	9.26
9.86wt.%Fe-B/WCNTs <sup>3d</sup>	-	298	Without light	4345.6	97.0	15.2	67.2
NiIr <sub>0.059</sub> /Al <sub>2</sub> O <sub>3</sub> <sup>4a</sup>	-	303	Without light		99.0	12.5	0.21

CoB <sub>0.358</sub> N <sub>0.286</sub> H <sub>0.251</sub> nanowires <sup>4f</sup>	-	293	Without light	2240.0	100.0	17	76.0
Rh-Cu nanoframe <sup>5h</sup>	-	298	Without light	44.8	31.4	300	0.56
Rh <sub>2</sub> Ni octahedrons <sup>7a</sup>	-	293	Without light	2195.2	100	21	15.7
NiFe <sup>2e</sup>	-	298	Without light	89.6	100.0	190	-
In situ Ni <sub>0.6</sub> Pd <sub>0.4</sub> <sup>2f</sup>	-	298	Without light	71.7	80.0	300	-
In situ Rh <sub>4.69</sub> Ni/graphene <sup>6a</sup>	-	298	Without light	89.6	100.0	49	1.91
NiMoB-La(OH) <sub>3</sub> <sup>3f</sup>	-	323	Without light	136.0	100.0	15	0.24
Amorphous Ni <sub>0.9</sub> Pt <sub>0.1</sub> /Ce <sub>2</sub> O <sub>3</sub> <sup>3g</sup>	-	298	Without light	172.0	100.0	43	0.47
Rh/Ni@SiO <sub>2</sub> <sup>4c</sup>	-	298	Without light	91.7	99.4	90	1.1
Ni <sub>64</sub> Pt <sub>36</sub> /MIL-96 <sup>4j</sup>	-	298	Without light	141.4	100.0	12	1.91
Ni <sub>88</sub> Pt <sub>12</sub> @MIL-101 <sup>4d</sup>	-	298	Without light	87.8	100.0	42	1.09
Ni <sub>0.6</sub> Fe <sub>0.4</sub> Mo <sup>4e</sup>	-	323	Without light	89.6	100.0	15	0.48
In situ RhNiB <sup>4h</sup>	-	298	Without light	89.6	100.0	22	-

Rh <sub>58</sub> Ni <sub>42</sub> @MIL-101 <sup>4i</sup>	-	323	Without light	141.4	100.0	7	5.73
Ni <sub>87</sub> Pt <sub>13</sub> /meso-Al <sub>2</sub> O <sub>3</sub> <sup>5a</sup>	-	323	Without light	89.6	100.0	5	2.67
Ni-0.080CeO <sub>2</sub> <sup>5b</sup>	-	323	Without light	71.7	99.0	10	0.86
Ni <sub>85</sub> Ir <sub>15</sub> @MIL-101 <sup>5c</sup>	-	298	Without light	-	100.0	-	0.4
Pt <sub>0.6</sub> Ni <sub>0.4</sub> /PDA-Rgo <sup>2h</sup>	-	293	Without light	-	100.0	3.5	11.43
Ni <sub>84</sub> Pt <sub>16</sub> /graphene <sup>5e</sup>	-	298	Without light	87.8	100.0	42	2.22
Ni@NiePt/La <sub>2</sub> O <sub>3</sub> <sup>5f</sup>	-	323	Without light	-	100.0	2.6	5.20
Ni <sub>30</sub> Fe <sub>30</sub> Pd <sub>40</sub> <sup>5g</sup>	-	323	Without light	224.0	100.0	27	0.36
Rh <sub>55</sub> Ni <sub>45</sub> /Ce(OH)CO <sub>3</sub> <sup>5i</sup>	-	303	Without light	8.87	100.0	15.6	2.5
octahedral PtNi <sup>5j</sup>	-	323	Without light	-	100.0	-	3.5
Ni <sub>37</sub> Pt <sub>63</sub> /g-C <sub>3</sub> N <sub>4</sub> <sup>5k</sup>	-	323	Without light	-	100.0	-	9.5
(Ni <sub>3</sub> Pt <sub>7</sub> ) <sub>0.5</sub> -(MnOx) <sub>0.5</sub> /NPC-900 <sup>5l</sup>	-	323	Without light	89.6	100.0	-	11.8

\* wavelength  $\lambda > 420$  nm, Xe lamp with a power density of 95 mW cm<sup>-2</sup>.

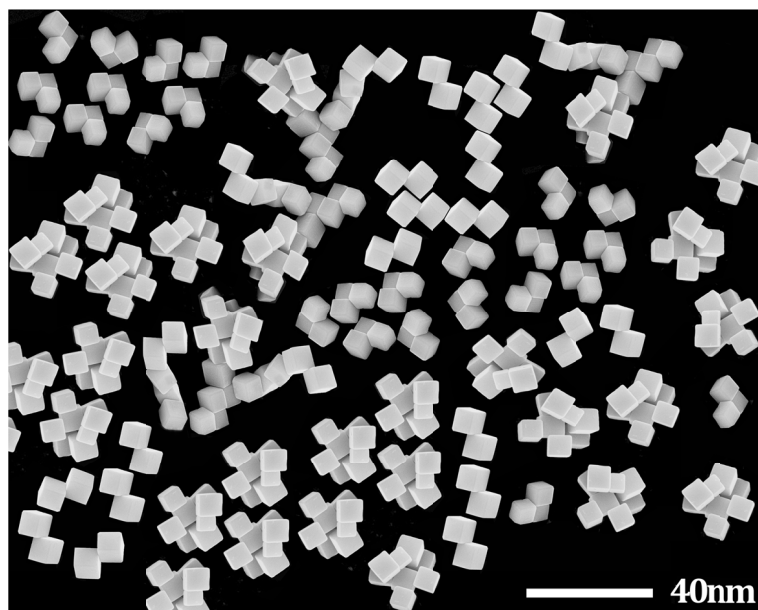


**Figure S1.** Typical low magnification STEM image of the as-prepared 6.8 nm fcc In NCs in this work.

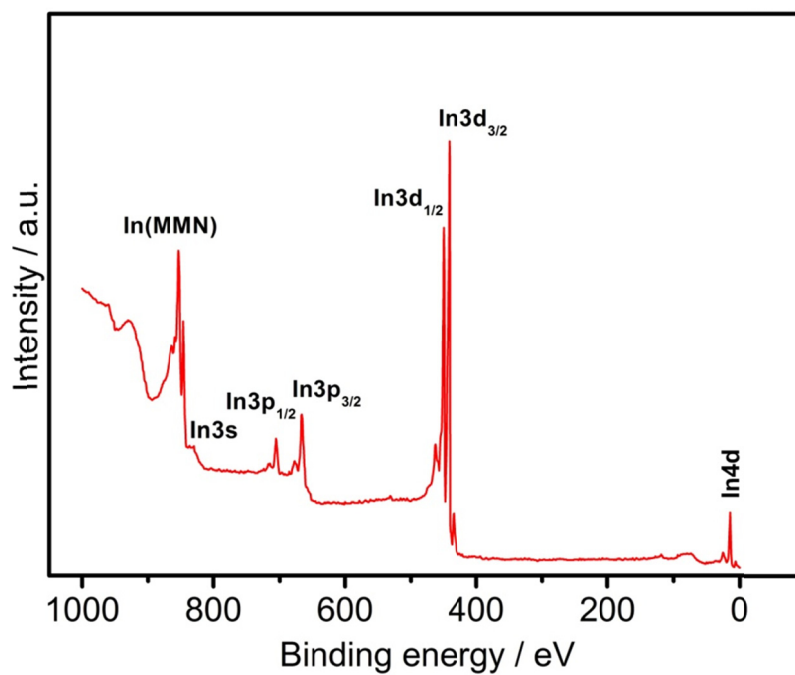


**Figure S2.** Overall XPS spectrum of the as-prepared 6.8 nm fcc In NCs in this work.

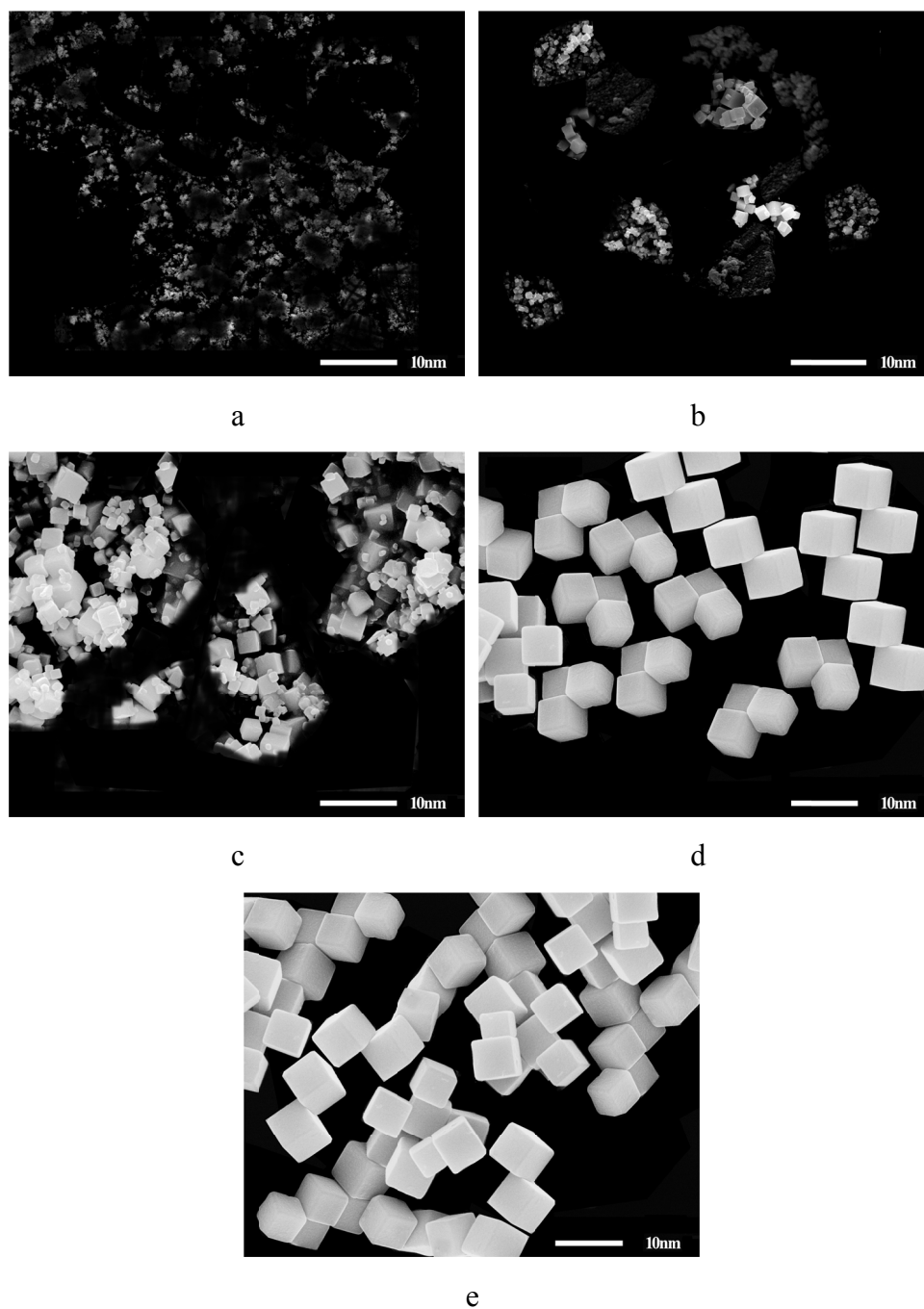


**Figure S3.** STEM images of the fcc In NCs prepared during SPT: (a) 1 min; (b) 4 min; (c) 7 min; (d) 10 min; (e) 30 min; (f) the sample of (d) after treated via SPT in the solution of choline and urea (mole ratio =1:2).

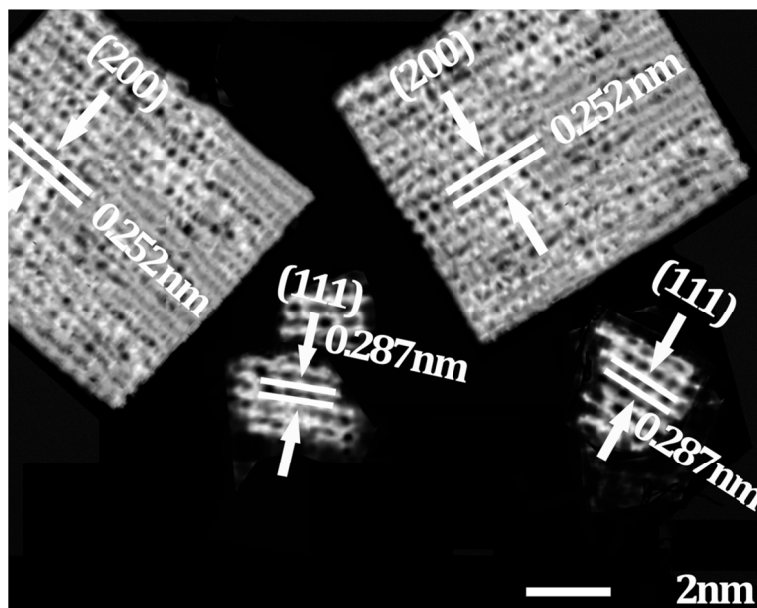


**Figure S4.** HR-STEM images of the In nanoclusters found during the synthesis of fcc In nanocubes during SPT.

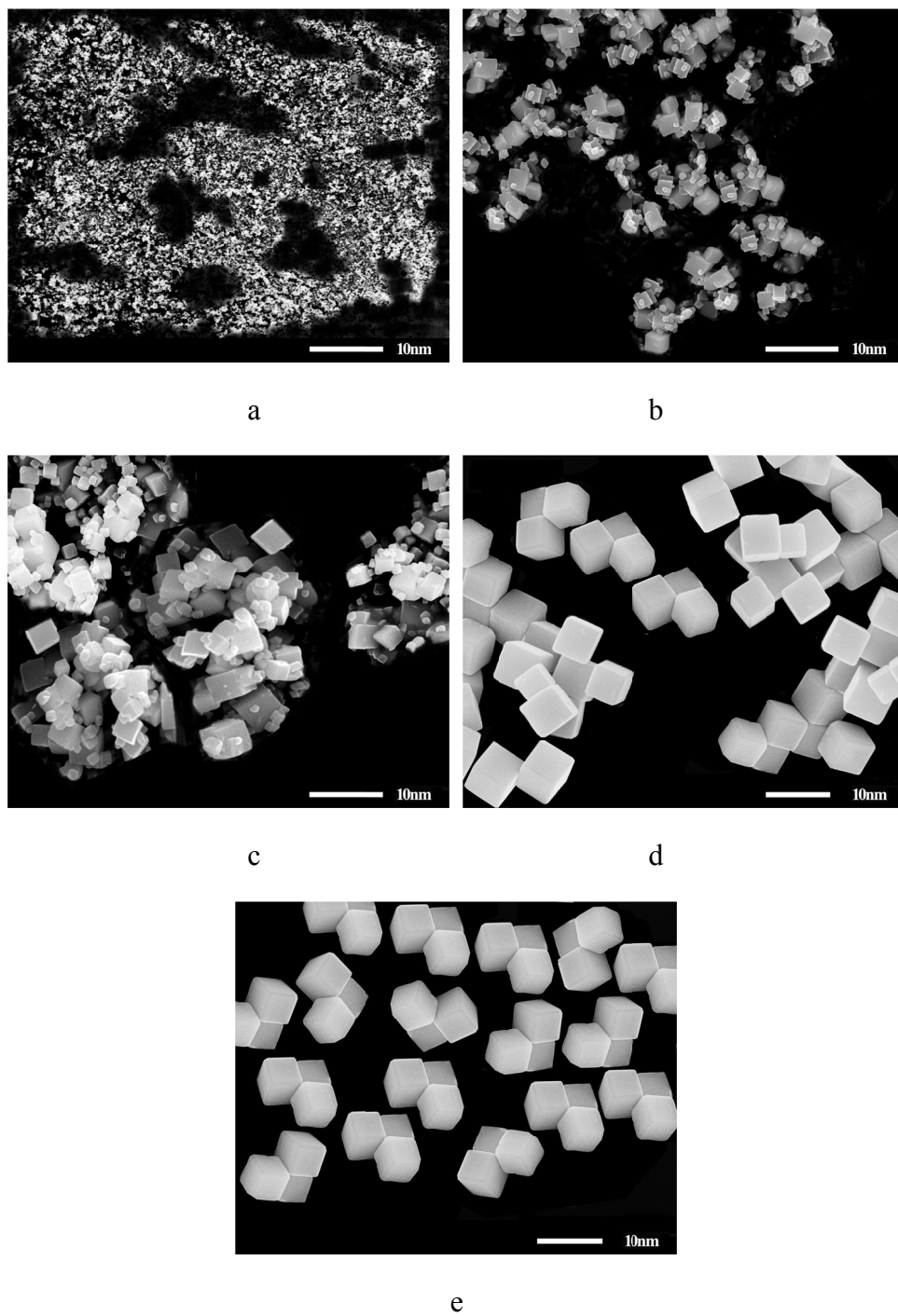
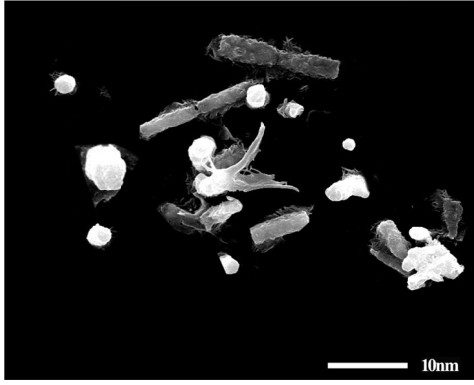
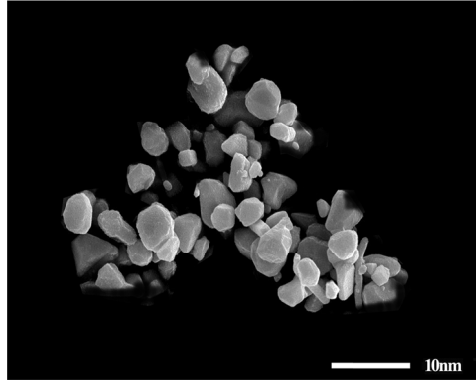


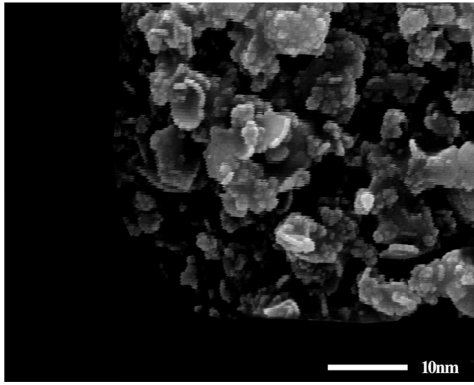
**Figure S5.** STEM images of the fcc In NCs obtained with different amounts of  $\text{KClO}_4$ : (a) 0 mmol, (b) 0.1 mmol, (c) 0.3 mmol, (d) 0.5 mmol, (e) 1.0 mmol.



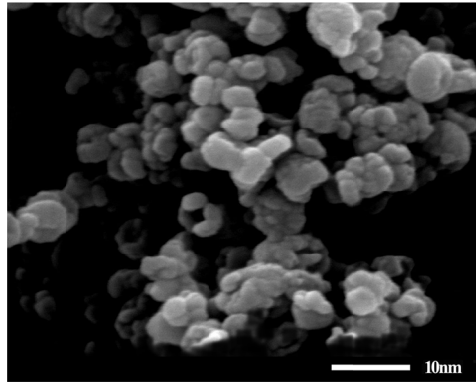
a



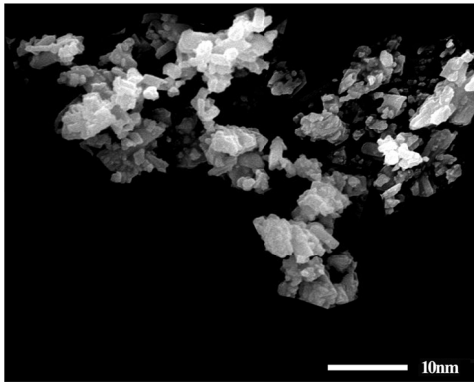
b



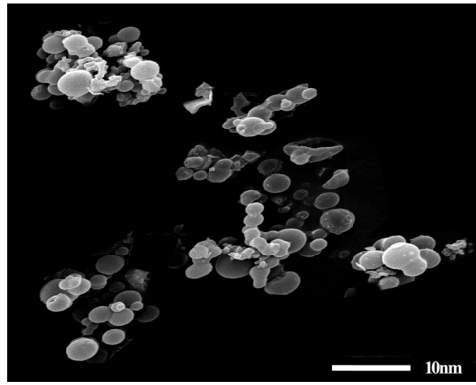
c



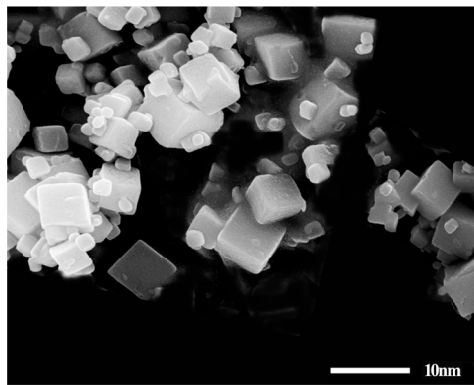
d



e



f



g

**Figure S6.** STEM images of the fcc In NCs prepared by SPT with (a)  $\text{NaNO}_3$ ; (b)  $\text{Na}_3\text{PO}_3$ ; (c)  $\text{Na}_3\text{PO}_4$ ; (d)  $\text{K}_2\text{SO}_4$ ; (e)  $\text{KBr}$ ; (f)  $\text{KI}$ ; (g) (a)–(e) after additional of  $\text{KClO}_4$ .

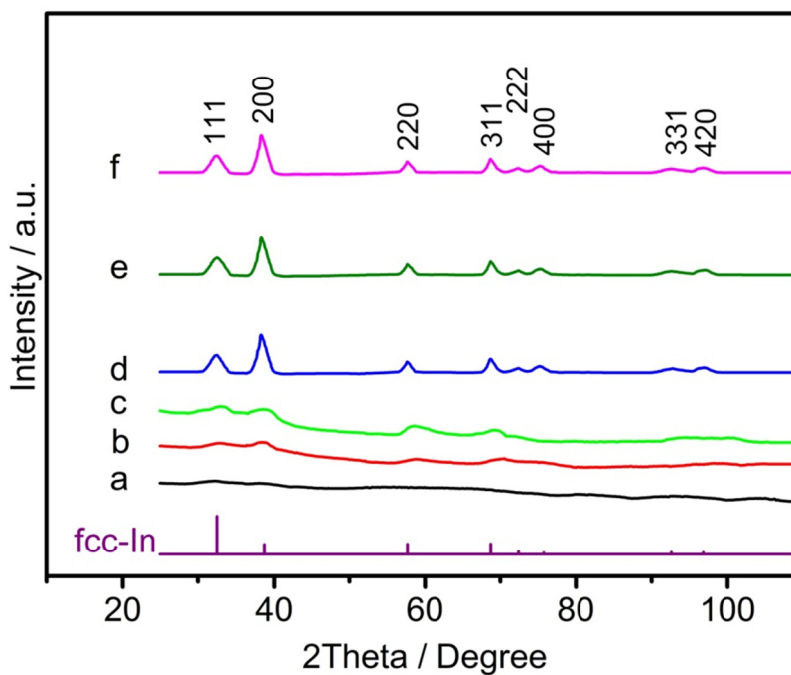


**Figure S7.** XRD patterns of the fcc In NCs prepared during SPT: (a) 1 min; (b) 4 min; (c) 7 min; (d) 10 min; (e) 30 min; (f) the sample of (d) after treated via SPT in the solution of choline and urea (mole ratio =1:2).

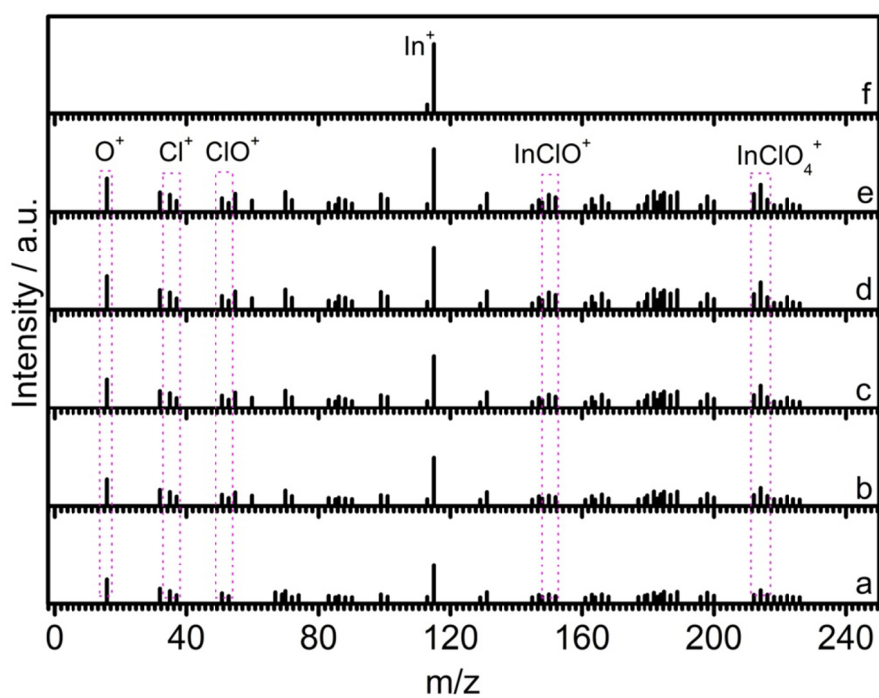


**Figure S8.** ToF-SIMS spectra of the fcc In NCs prepared during SPT: (a) 1 min; (b) 4 min; (c) 7 min; (d) 10 min; (e) 30 min; (f) the sample of (d) after treated via SPT in the solution of choline and urea (mole ratio =1:2).

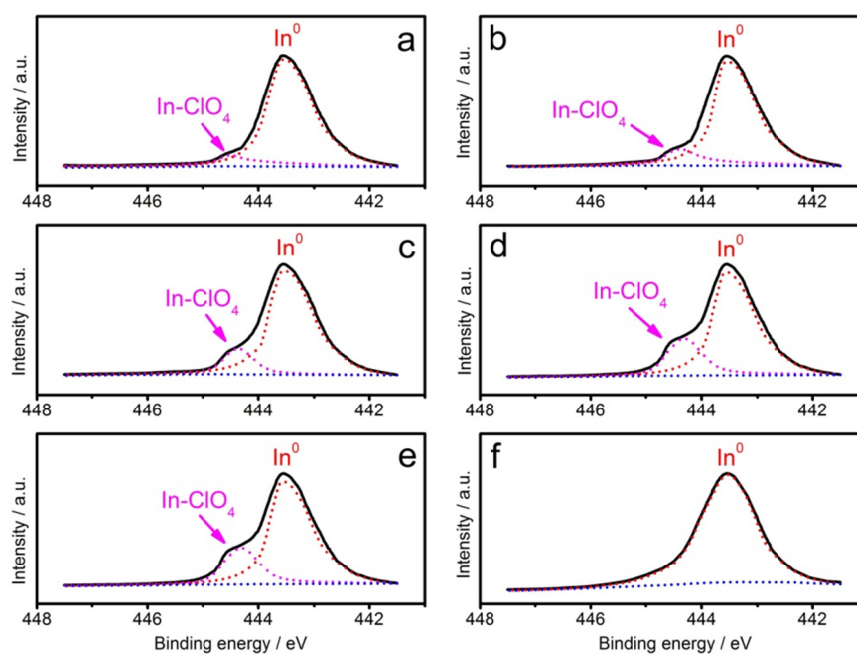


**Figure S9.** In  $3d_{5/2}$  spectra of the fcc In NCs prepared during SPT: (a) 1 min; (b) 4 min; (c) 7 min; (d) 10 min; (e) 30 min; (f) the sample of (d) after treated via SPT in the solution of choline and urea (mole ratio =1:2).

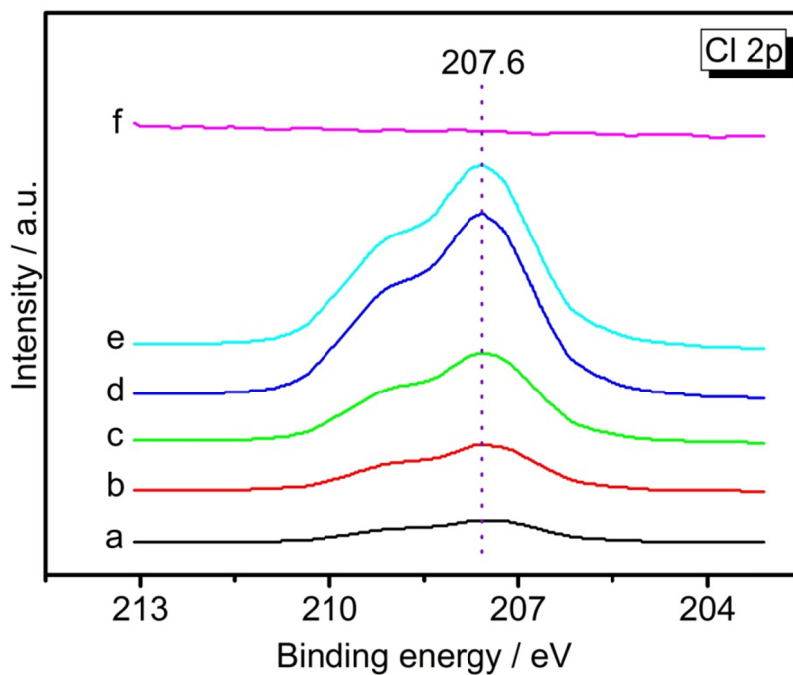


**Figure S10.** Cl2p spectra of the fcc In NCs prepared during SPT: (a) 1 min; (b) 4 min; (c) 7 min; (d) 10 min; (e) 30 min; (f) the sample of (d) after treated via SPT in the solution of choline and urea (mole ratio =1:2).

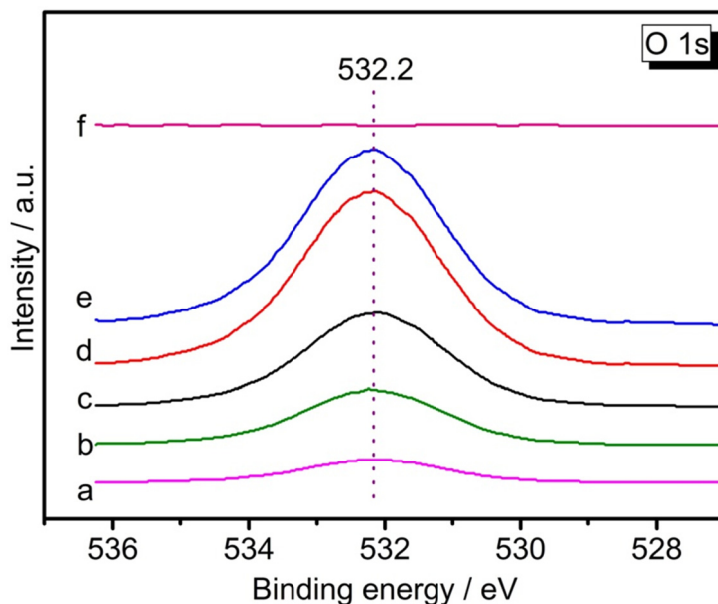


**Figure S11.** O1s spectra of the fcc In NCs prepared during SPT: (a) 1 min; (b) 4 min; (c) 7 min; (d) 10 min; (e) 30 min; (f) the sample of (d) after treated via SPT in the solution of choline and urea (mole ratio =1:2).

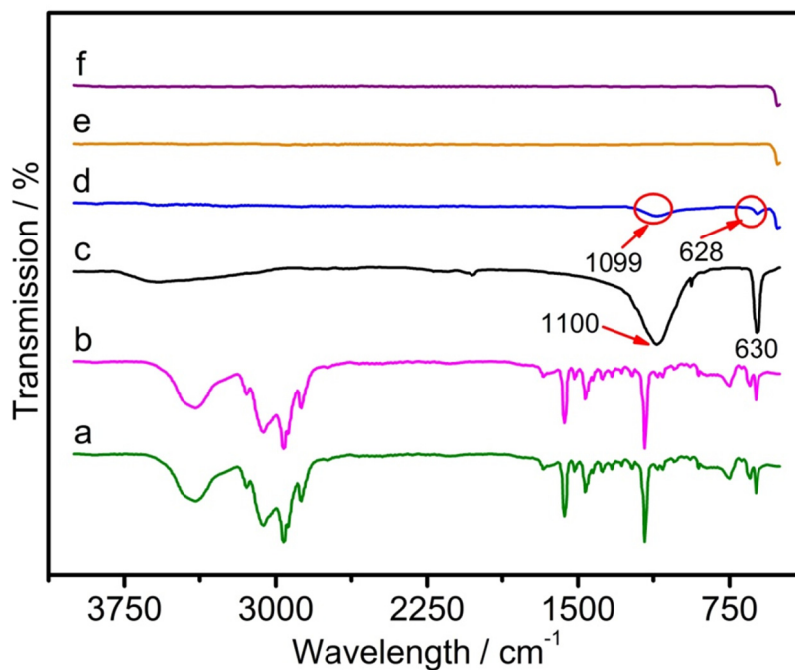


**Figure S12.** FT-IR spectra of (a) [BMIM]Cl; (b) the recycled [BMIM]Cl after the SPT reaction; (c) commercial KClO<sub>4</sub>; (d) the as-prepared fcc In NCs only washed with water; (e) the (d) sample further treated with the solution of choline and urea (mole ratio =1:2) via SPT; (f) the conventional fcc In NCs.

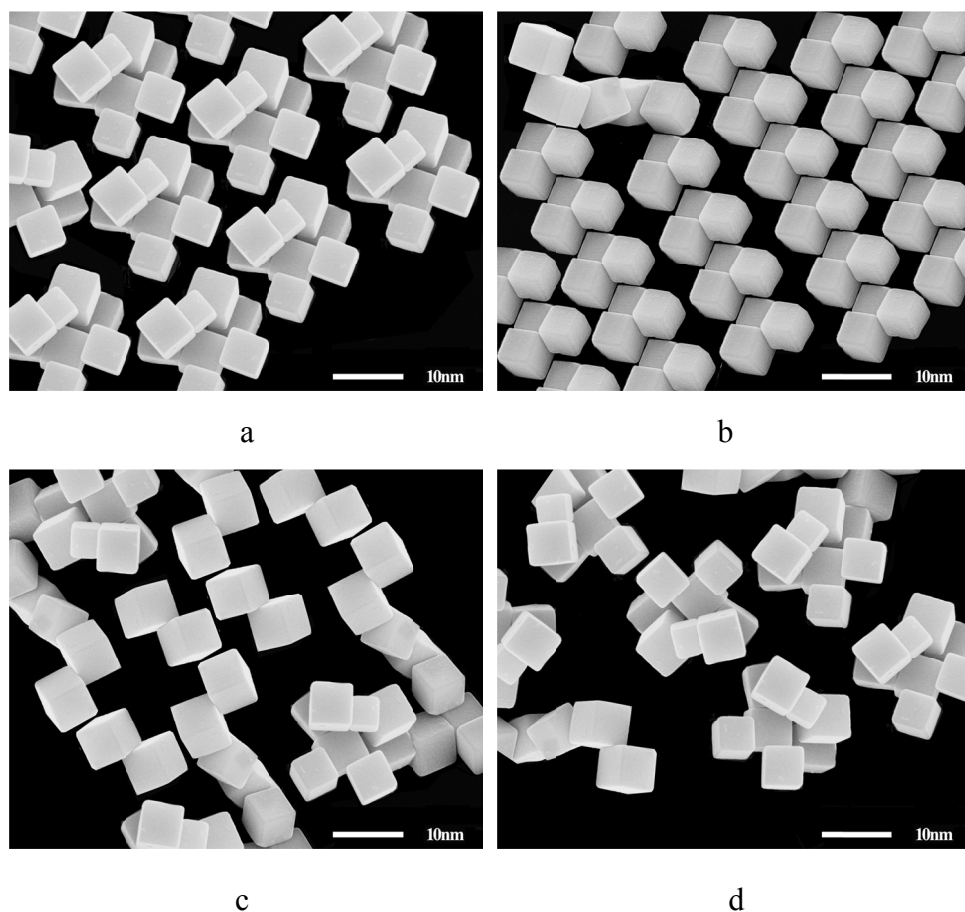


**Figure S13.** STEM images of fcc In NCs prepared with (a) 30 mL [BMIM] [BF<sub>4</sub>]; (b) 30 mL [BMIM][PF<sub>6</sub>]; (c) 50 mL [BMIM]Cl; (d) 100 mL [BMIM]Cl.

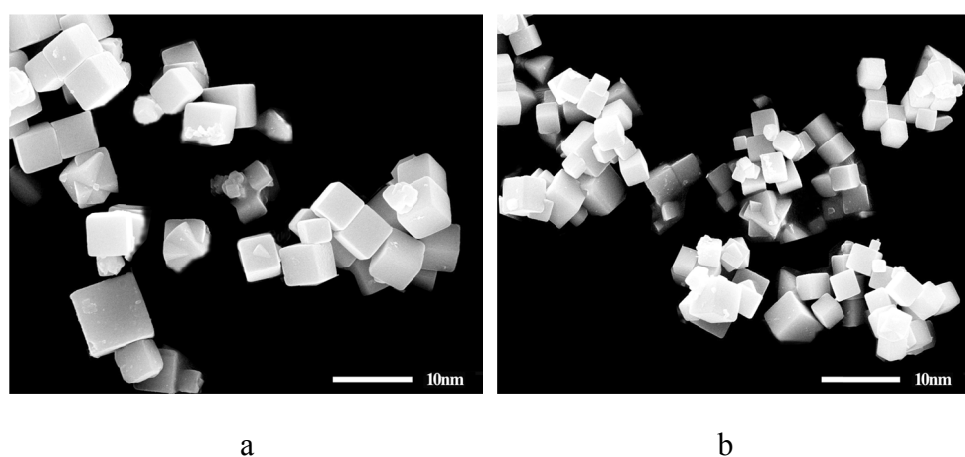


**Figure S14.** STEM images of the fcc In NCs prepared with (a) In(CH<sub>3</sub>CO<sub>2</sub>)<sub>3</sub> and (b) In(acac)<sub>3</sub> as the precursors, respectively.

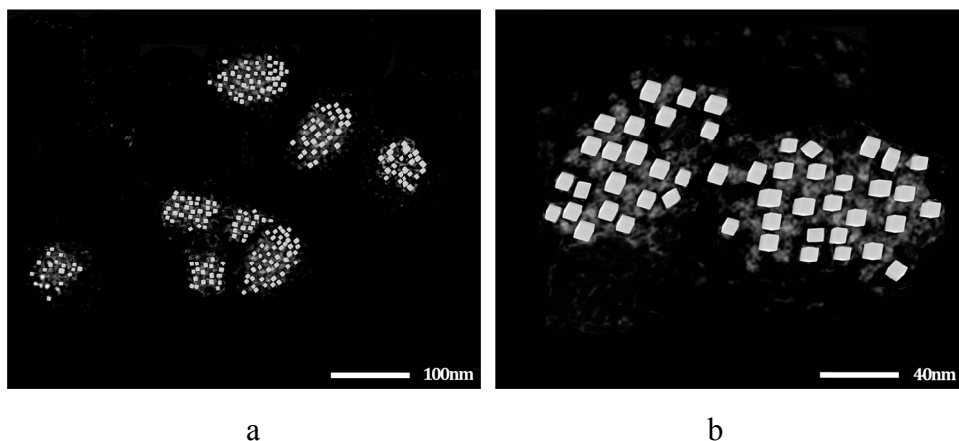


**Figure S15.** (a) Low magnification and (b) enlarged STEM images of 133 mg catalysts of 6.8 nm fcc In nanocubes loaded on C (80 wt.%).

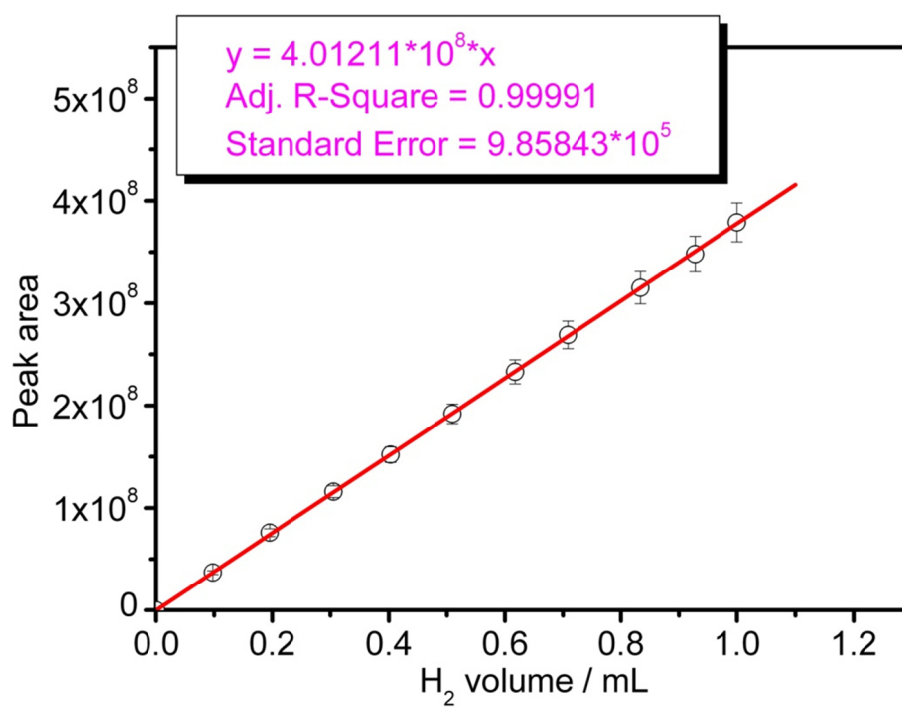


**Figure S16.** The H<sub>2</sub> calibration curves for the quantitative analysis of gas products by the on-line gas chromatography system (GC) equipped with a thermal conductivity detector (TCD).

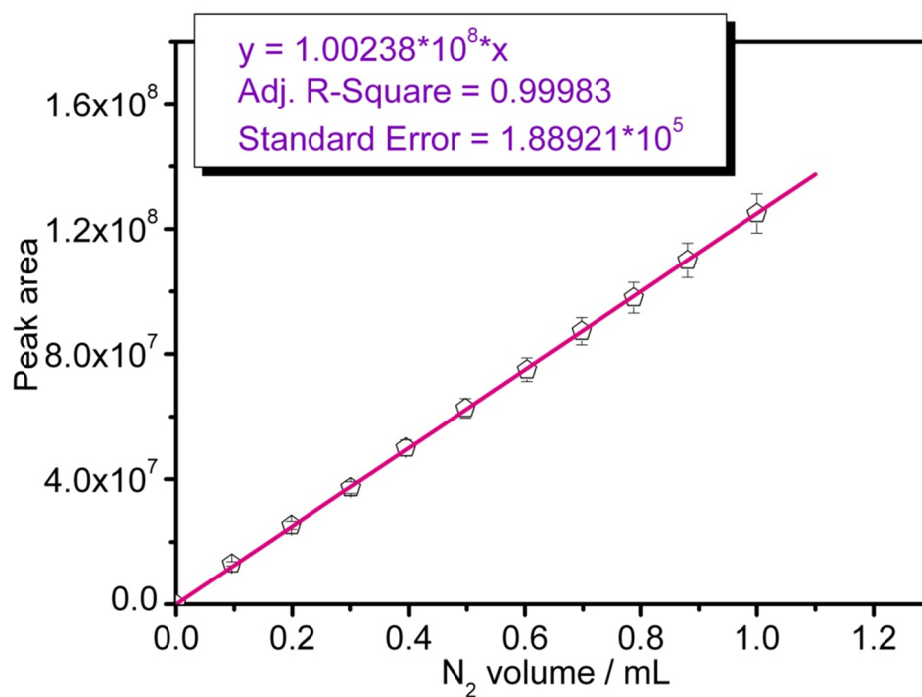


**Figure S17.** The N<sub>2</sub> calibration curves for the quantitative analysis of gas products by the on-line gas chromatography system (GC) equipped with a thermal conductivity detector (TCD).

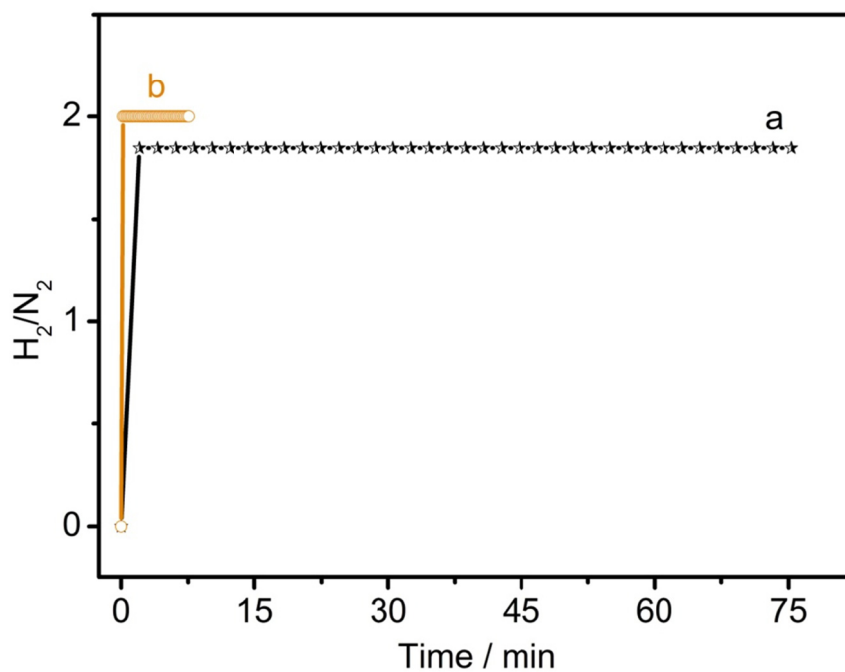


**Figure S18.** Plots of H<sub>2</sub>/N<sub>2</sub> ratio versus time during the 100 mL N<sub>2</sub>H<sub>4</sub> aqueous solution decomposition over 6.8 nm fcc In nanocubes loaded on C (80 wt.%) : (a) without light and (b) with light. ([catalyst]= 1.33 gL<sup>-1</sup>; [N<sub>2</sub>H<sub>4</sub>] = 5.0 molL<sup>-1</sup>; wavelength  $\lambda > 420$  nm, Xe lamp with a power density of 95 mW cm<sup>-2</sup>).

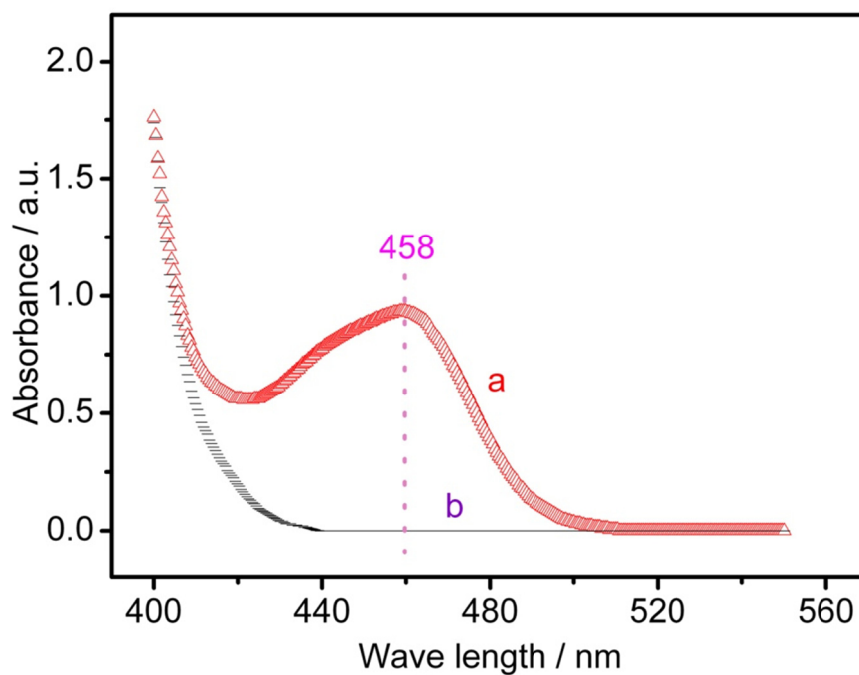


**Figure S19.** Typical UV-Vis spectra of hydrous hydrazine (a) before and (b) after the completion of hydrazine decomposition reaction over 6.8 nm fcc-In nanocubes loaded on C (80 wt.%) ( $[\text{catalyst}] = 1.33 \text{ gL}^{-1}$ ;  $[\text{N}_2\text{H}_4] = 5.0 \text{ molL}^{-1}$ ; wavelength  $\lambda > 420 \text{ nm}$ , Xe lamp with a power density of  $95 \text{ mW cm}^{-2}$ ). For the measurement, a mixture of 0.5000 g of para-dimethylaminobenzaldehyde, 25.00 mL of ethanol, and 2.50 mL of hydrochloric acid ( $1.000 \text{ mol L}^{-1}$ ) was used as the chromogenic agent for  $\text{N}_2\text{H}_4$ .

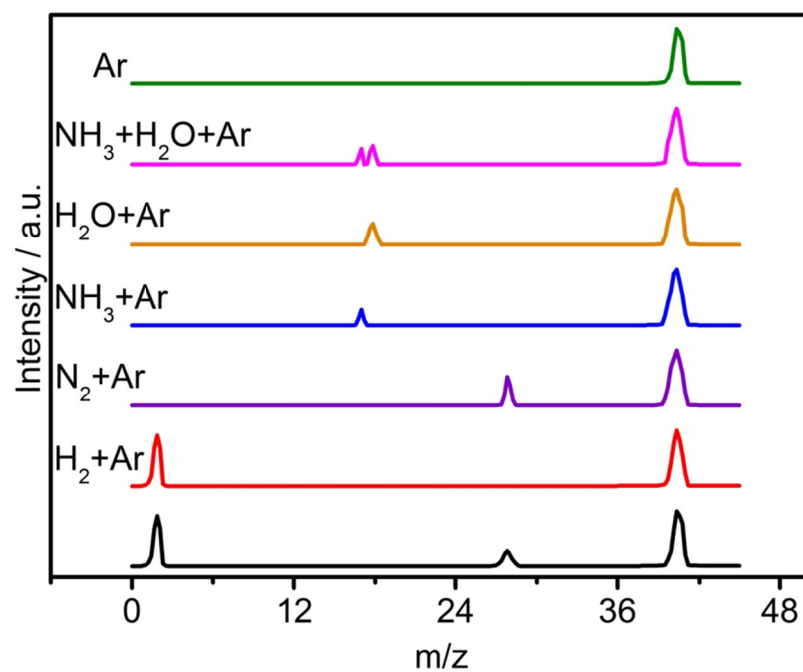


**Figure S20.** Mass spectral (MS) profile of the gases released from the complete decomposition of hydrous hydrazine at room temperature over 6.8 nm fcc-In nanocubes loaded on C (80 wt.%) ( $[\text{catalyst}] = 1.33 \text{ gL}^{-1}$ ;  $[\text{N}_2\text{H}_4] = 5.0 \text{ molL}^{-1}$ ; wavelength  $\lambda > 420 \text{ nm}$ , Xe lamp with a power density of  $95 \text{ mW cm}^{-2}$ ).

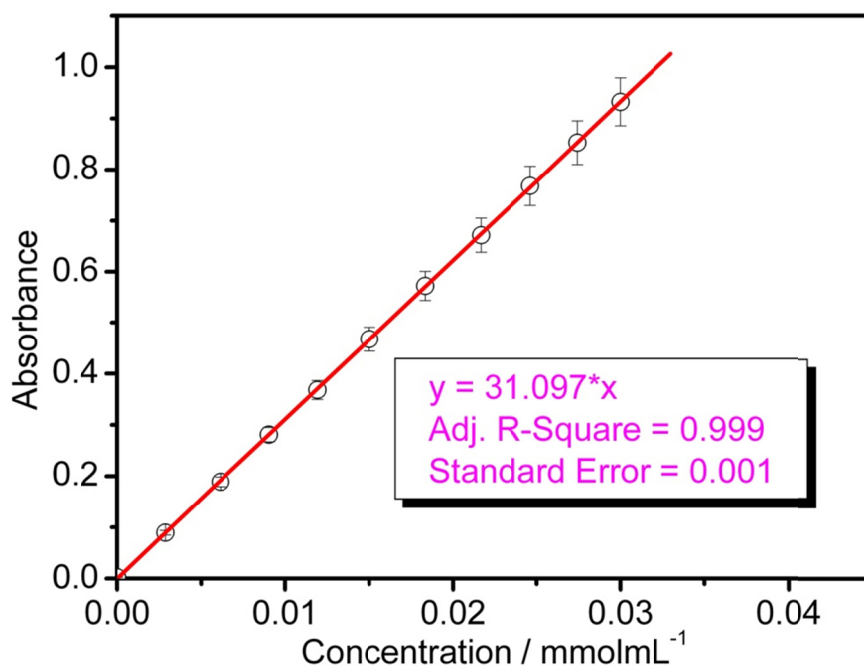


**Figure S21.** The calibration curves for the derivatized hydrazine in the UV assay at wavelength of 458 nm. For the measurement, a mixture of 0.5000 g of para-dimethylaminobenzaldehyde, 25.00 mL of ethanol, and 2.50 mL of hydrochloric acid (1.000 mol L<sup>-1</sup>) was used as the chromogenic agent for N<sub>2</sub>H<sub>4</sub>.

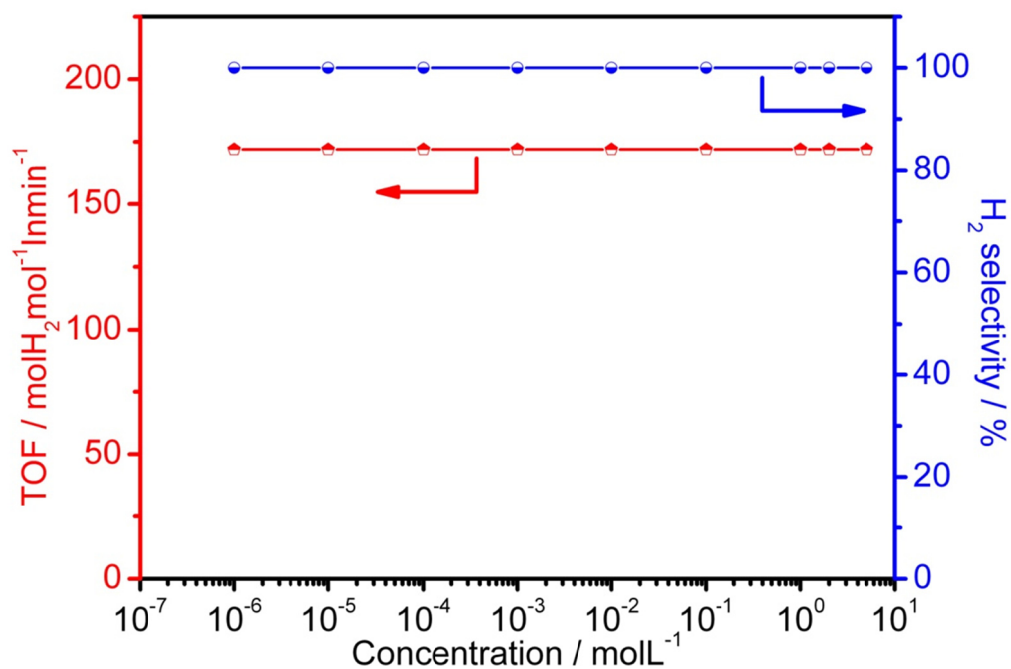


**Figure S22.** The variation of TOF and H<sub>2</sub> selectivity during the decomposition of hydrous hydrazine at room temperature over 6.8 nm fcc-In nanocubes loaded on C (80 wt.%) at different NaOH concentrations in light ([catalyst]= 1.33 gL<sup>-1</sup>; [N<sub>2</sub>H<sub>4</sub>] = 5.0 molL<sup>-1</sup>; wavelength  $\lambda > 420$  nm, Xe lamp with a power density of 95 mWcm<sup>-2</sup>).

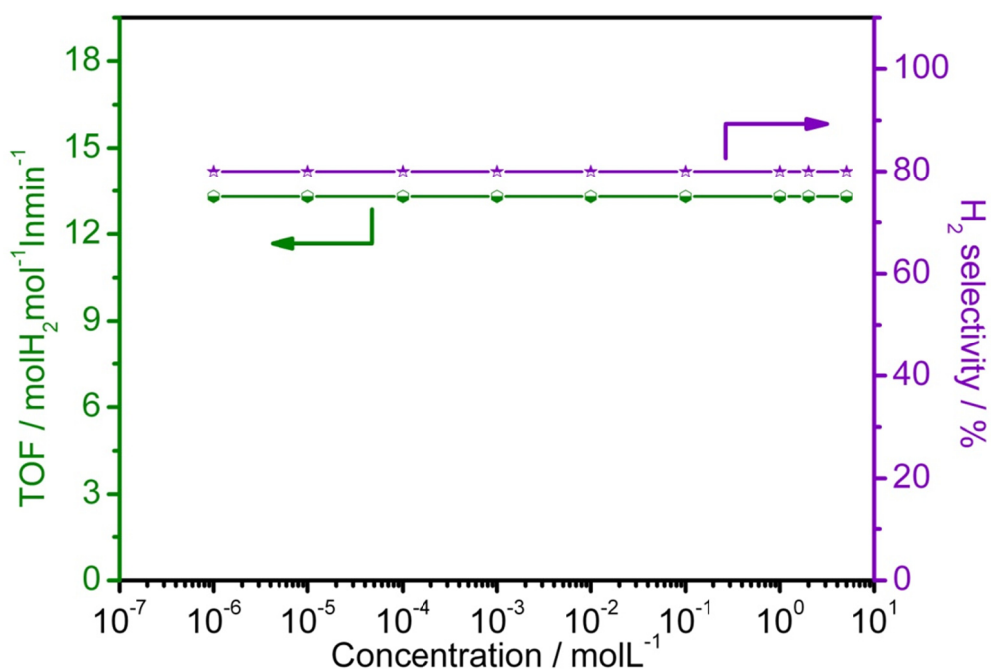


**Figure S23.** The variation of TOF and H<sub>2</sub> selectivity during the decomposition of hydrous hydrazine at room temperature over 6.8 nm fcc-In nanocubes loaded on C (80 wt.%) at different NaOH concentrations in dark ([catalyst]= 1.33 gL<sup>-1</sup>; [N<sub>2</sub>H<sub>4</sub>] = 5.0 molL<sup>-1</sup>).

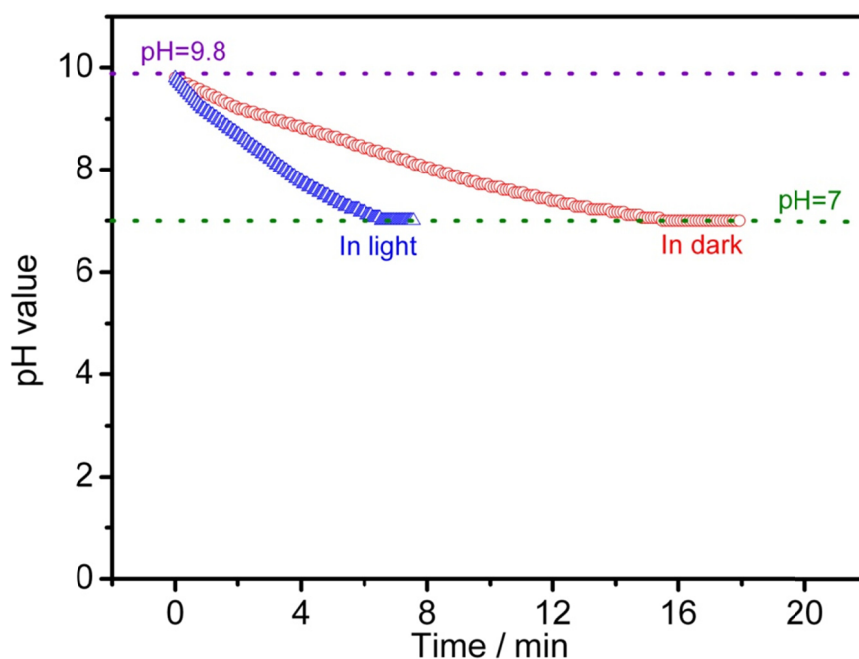


**Figure S24.** The pH monitoring during the decomposition of hydrous hydrazine at room temperature over 6.8 nm fcc-In nanocubes loaded on C (80 wt.%) in dark and in light.([catalyst]= 1.33 gL<sup>-1</sup>; [N<sub>2</sub>H<sub>4</sub>] = 5.0 molL<sup>-1</sup>; wavelength  $\lambda > 420$  nm, Xe lamp with a power density of 95 mWcm<sup>-2</sup>).

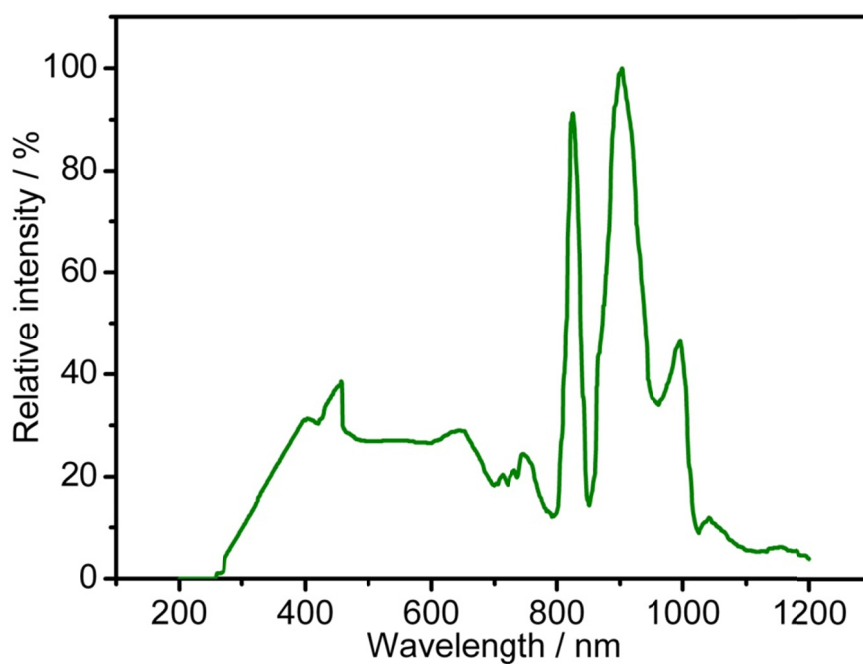


**Figure S25.** The spectrum of the 500 W Xe lamp used in our work.

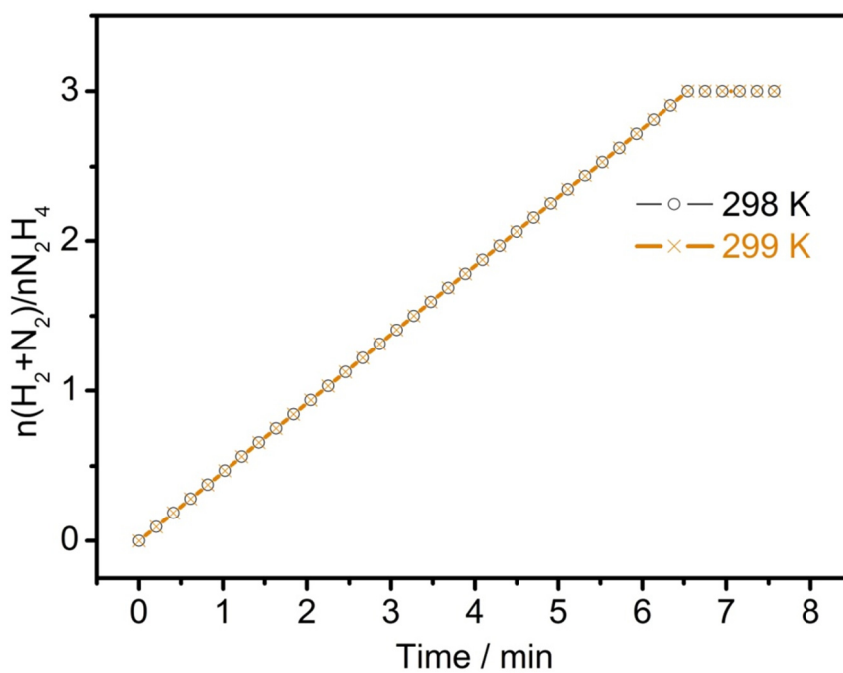


**Figure S26.** Time profiles for decomposition of 100 mL  $\text{N}_2\text{H}_4$  aqueous solution decomposition over 6.8 nm fcc In nanocubes loaded on C (80 wt.%) carried out at 298 and 299 K with light. ( $[\text{catalyst}] = 1.33 \text{ gL}^{-1}$ ;  $[\text{N}_2\text{H}_4] = 5.0 \text{ molL}^{-1}$ ; wavelength  $\lambda > 420 \text{ nm}$ , Xe lamp with a power density of  $95 \text{ mW cm}^{-2}$ )

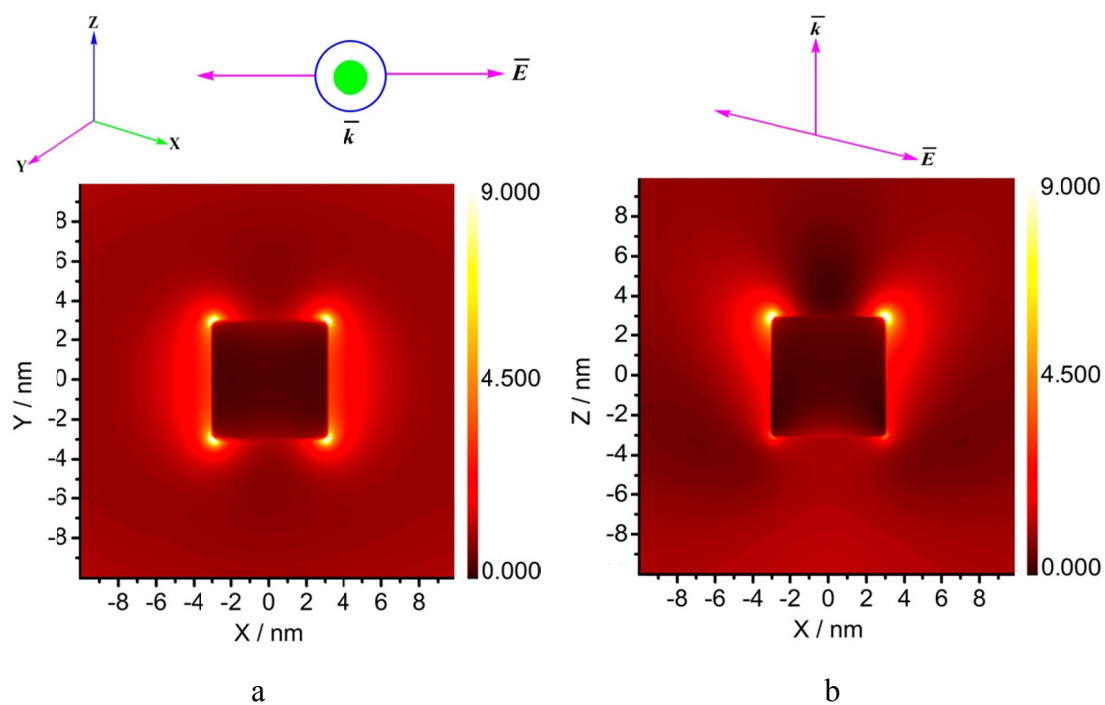


**Figure S27.** The typical simulated profiles of the electric field intensity ( $E^2 = E_x^2 + E_y^2 + E_z^2$ ) performed over the middle plane of the 6.8 nm In NCs along x-y plane (panel a) and x-z plane (panel b) under light. The result shows high field intensity taking place at the corners and edges of the nanocrystals. In nanocubes with precise shapes and sizes have been built up for the simulations as those shown in Figure 1.

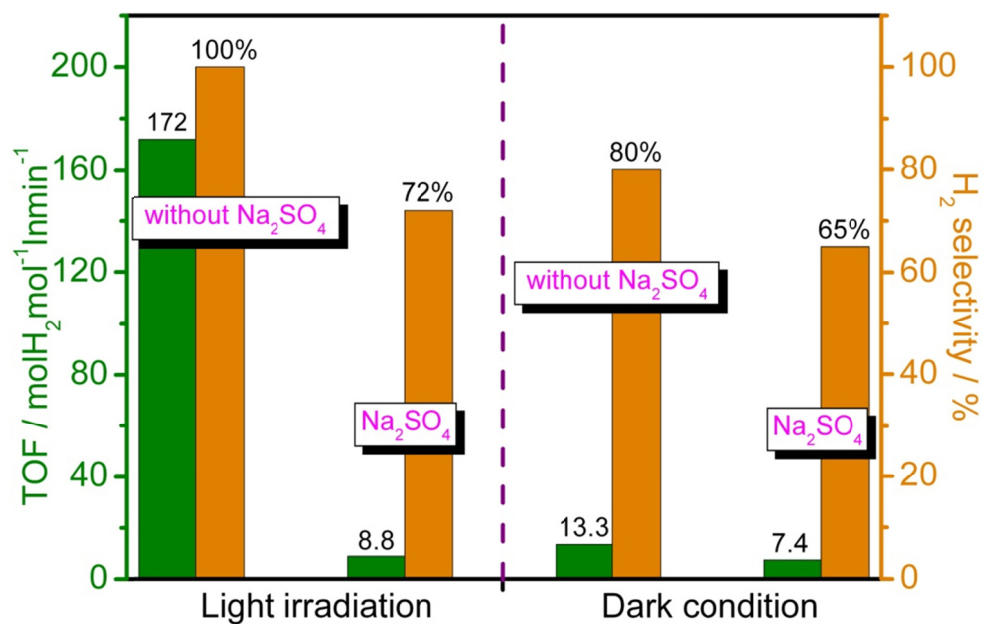


**Figure S28.** Comparison of the catalytic performance of the 6.8 nm In NCs towards aqueous hydrazine dehydrogenation under light irradiation ( $\lambda > 420$  nm) and dark condition in the absence or presence of 5 mmol Na<sub>2</sub>SO<sub>4</sub> as negative charge scavenger.

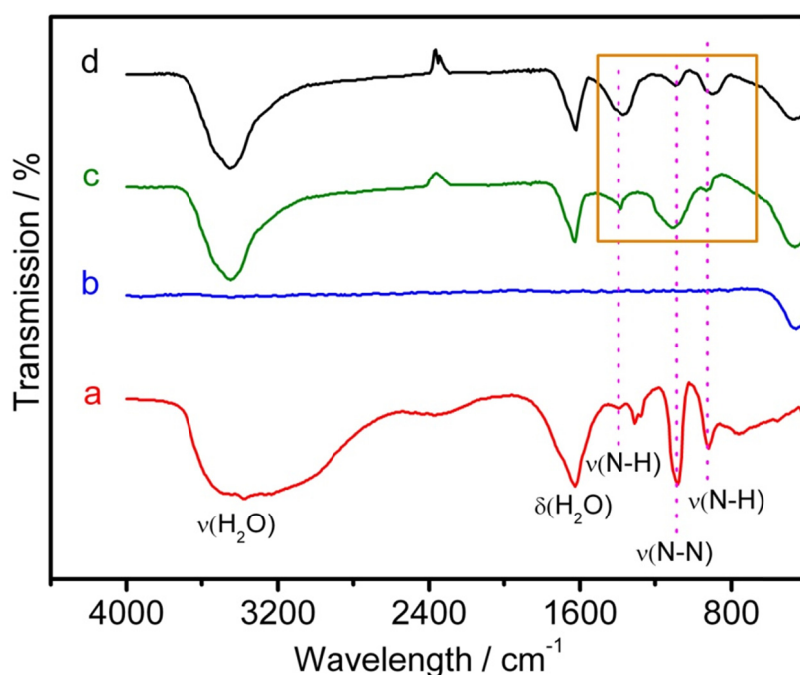


**Figure S29.** The ATR-FTIR of (a) aqueous hydrazine; (b) 6.8 nm fcc In nanocubes dispersed in water; (c) 6.8 nm fcc In nanocubes after addition of aqueous hydrazine in dark; (d) 6.8 nm fcc In nanocubes after addition of aqueous hydrazine in light.

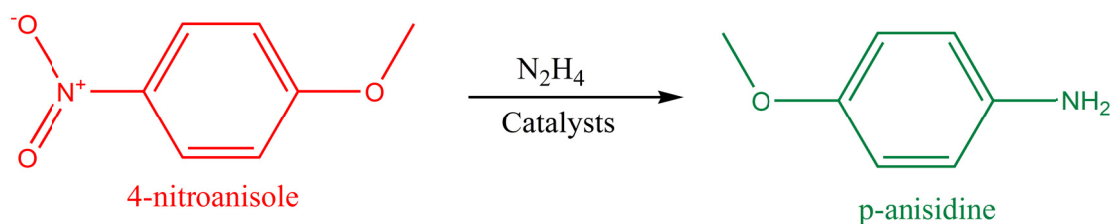


**Figure S30.** Scheme for the reduction of 4-nitroanisole by  $\text{N}_2\text{H}_4$  to *p*-anisidine in the presence of catalysts.

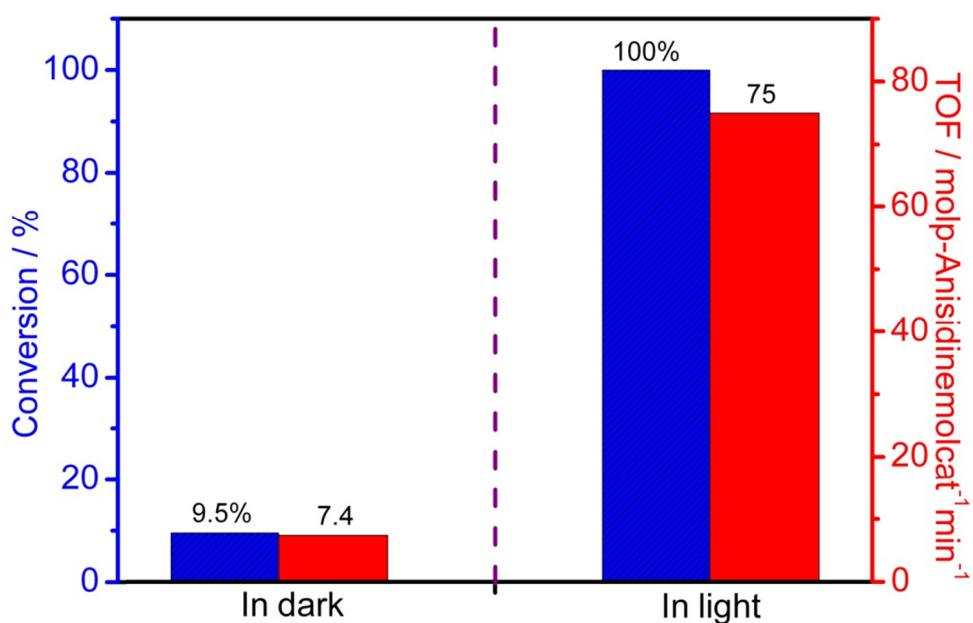


**Figure S31.** Conversion and TOF for the reduction of 4-nitroanisole by  $\text{N}_2\text{H}_4$  over 6.8 nm fcc In nanocubes loaded on C (80 wt.%) in dark and in light at 298K for 1h. ([catalyst]= 1.33  $\text{gL}^{-1}$ ; [ $\text{N}_2\text{H}_4$ ] = 5.0  $\text{molL}^{-1}$ ; [4-nitroanisole] = 2.5  $\text{molL}^{-1}$ ; wavelength  $\lambda > 420$  nm, Xe lamp with a power density of 95  $\text{mWcm}^{-2}$ ).

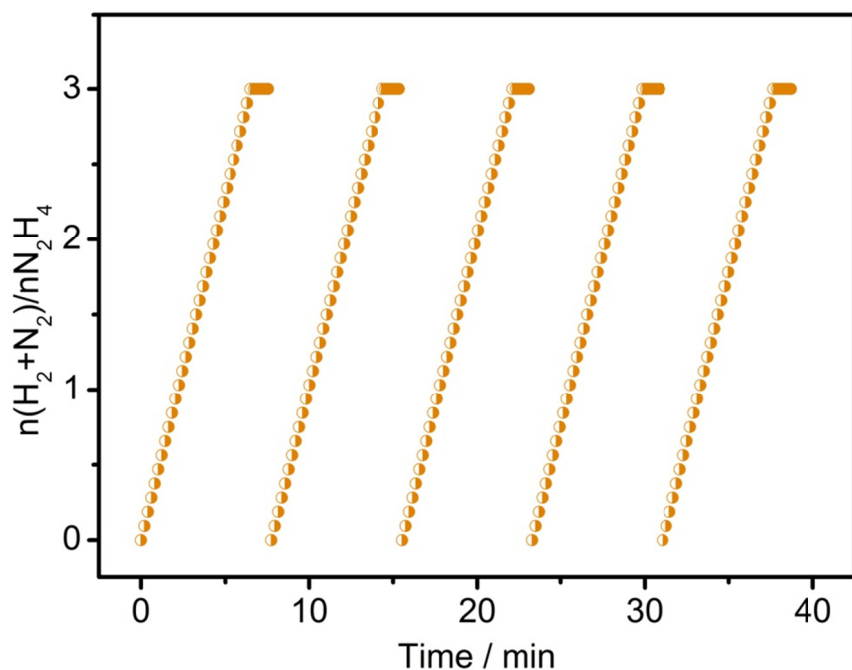


**Figure S32.** Time profiles of hydrogen generated from aqueous  $\text{N}_2\text{H}_4$  over 6.8 nm fcc In nanocubes loaded on C (80 wt.%) for five cycles of reusability test at 298 K with light. ([catalyst]=  $1.33 \text{ gL}^{-1}$ ;  $[\text{N}_2\text{H}_4] = 5.0 \text{ molL}^{-1}$ ; wavelength  $\lambda > 420 \text{ nm}$ , Xe lamp with a power density of  $95 \text{ mW cm}^{-2}$ )

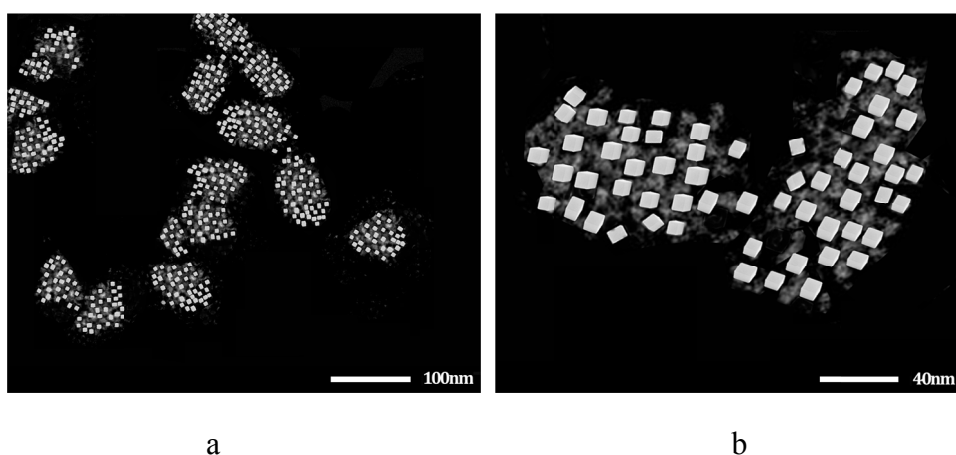


**Figure S33.** (a) Low magnification and (b) enlarged STEM images of 6.8 nm fcc In nanocubes loaded on C (80 wt.%) after five cycles. ([catalyst]=  $1.33 \text{ gL}^{-1}$ ;  $[\text{N}_2\text{H}_4] = 5.0 \text{ molL}^{-1}$ ; wavelength  $\lambda > 420 \text{ nm}$ , Xe lamp with a power density of  $95 \text{ mW cm}^{-2}$ )

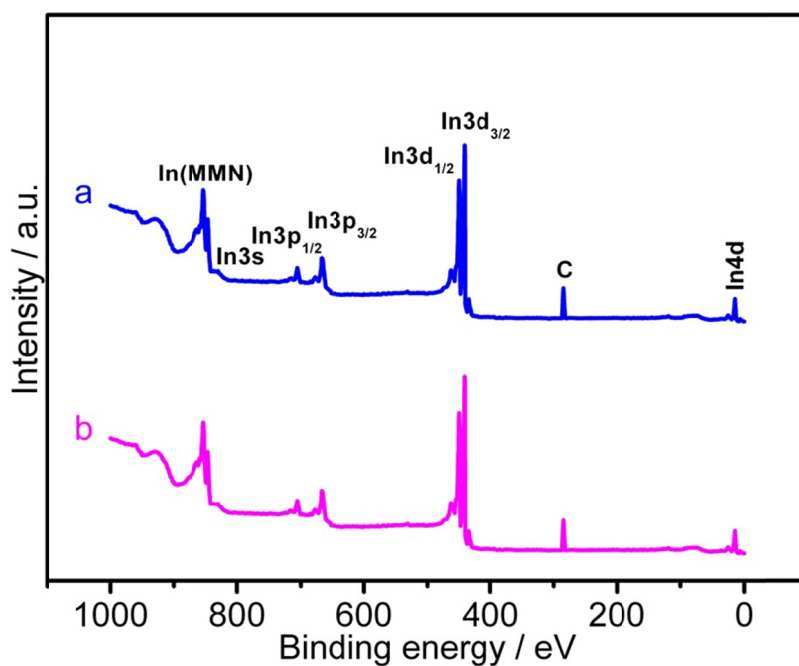


**Figure S34.** Overall XPS spectra of 6.8 nm fcc In nanocubes loaded on C (80 wt.%) (a) before and (b) after five cycles in this work.

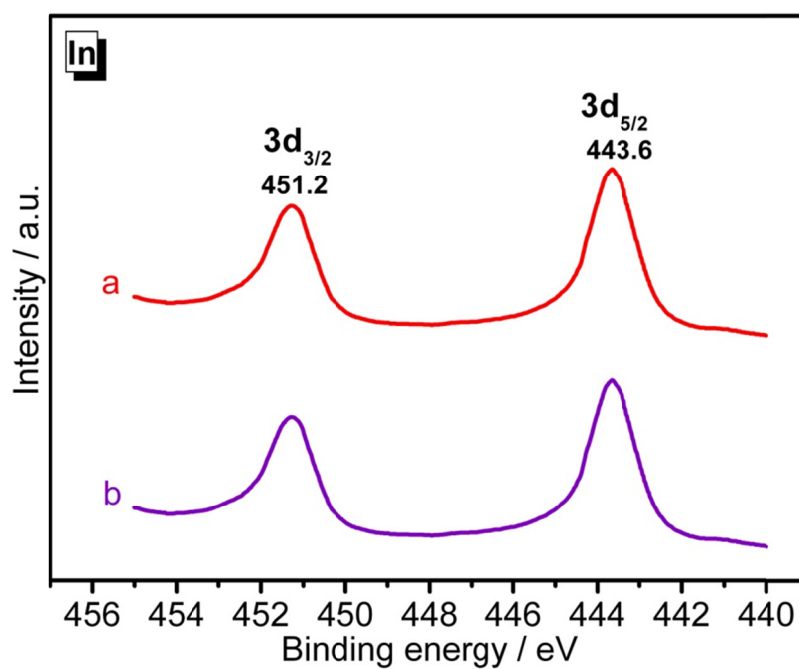


**Figure S35.** In3d XPS spectra of 6.8 nm fcc In nanocubes loaded on C (80 wt.%) (a) before and (b) after five cycles in this work.

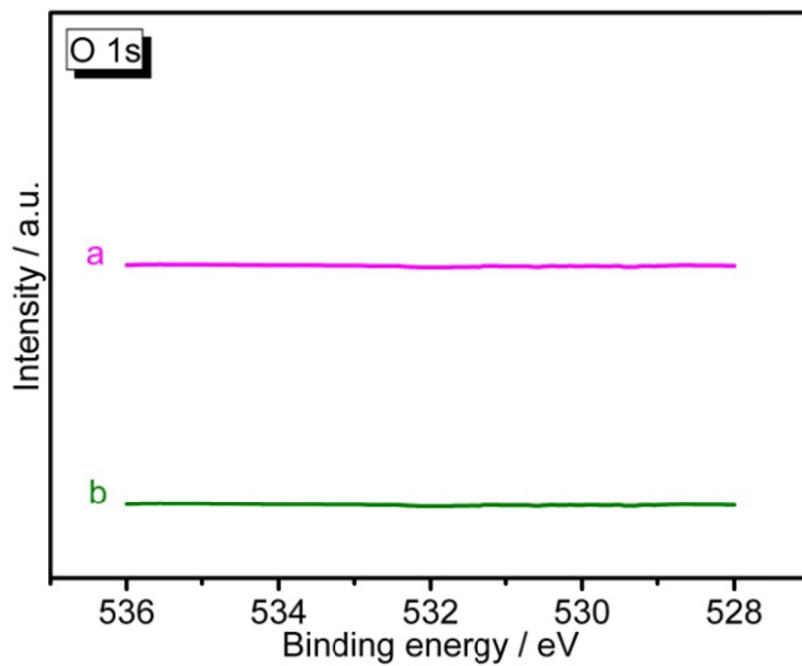


**Figure S36.** O1s XPS spectra of 6.8 nm fcc In nanocubes loaded on C (80 wt.%) (a) before and (b) after five cycles in this work.

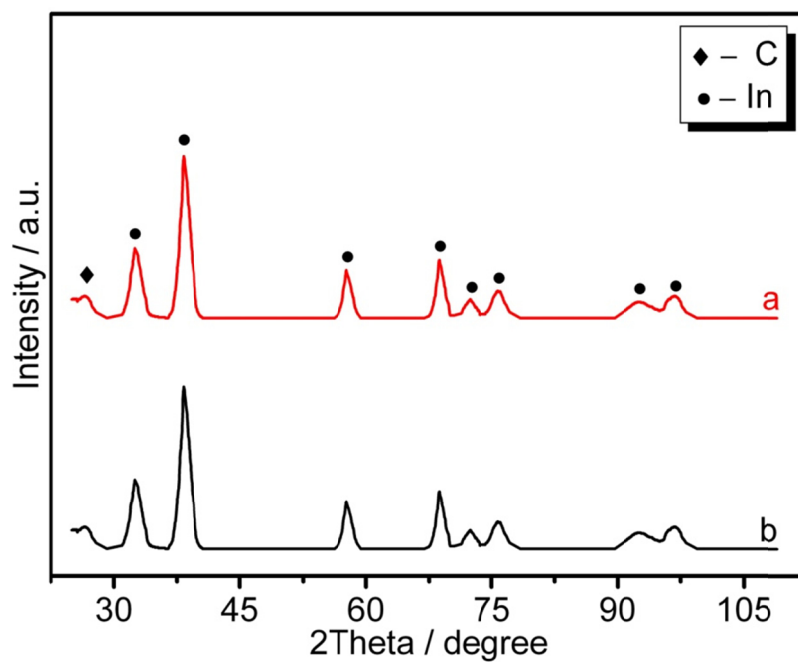


**Figure S37.** XRD profiles of 6.8 nm fcc In nanocubes loaded on C (80 wt.%) (a) before and (b) after five cycles in this work.